Published in final edited form as:

Biochemistry. 2018 June 26; 57(25): 3480–3492. doi:10.1021/acs.biochem.8b00223.

The structural basis of the molecular switch between phosphatase and mutase functions of human phosphomannomutase 1 under ischemic conditions

Tianyang Ji[1], **Chunchun Zhang**[2,3], **Li Zheng**[2], **Debra Dunaway-Mariano**[2], **Karen N. Allen**[1]

[1]Boston University, Department of Chemistry, Boston, MA, USA

[2]University of New Mexico, Department of Chemistry and Chemical Biology, Albuquerque, NM, USA

[3]Current address: Testing and Analytical Center, Sichuan University, Chengdu, Sichuan 610064, P.R. China

Abstract

The human phosphomannomutases PMM1 and PMM2 catalyze the interconversion of hexose 6-phosphates and hexose 1-phosphates. The two isoforms share 66% sequence identity and have similar kinetic properties as mutases *in vitro*, but differ in their functional roles *in vivo*. Though the physiological role of PMM2 is catalysis of the mutase reaction that provides the mannose 1-phosphate (Man-1-P) essential for protein glycosylation, PMM1 is thought to provide a phosphohydrolase activity in the presence of inosine monophosphate (IMP), converting glucose 1,6-bisphosphate (Glu-1,6-P_2) to glucose 6-phosphate (Glu-6-P), rescuing glycolysis during brain ischemia. To uncover the structural basis of how IMP binding converts PMM1 from a mutase to a phosphatase, the 1.93 Å resolution structure of PMM1 complexed with IMP was determined. The structure reveals IMP bound at the substrate recruitment site, thus inhibiting the mutase activity while simultaneous activating a phosphatase activity (IMP K_{act} = 1.5 μM) resulting from the hydrolysis of the phospho-enzyme. The bound structure and site-directed mutagenesis confirm that the long-range electrostatic interactions provided by Arg180 and Arg183 conserved in PMM1 are the major contributors to IMP binding, and their oblation removes phosphatase but not mutase activity. These residues are not present in the PMM2 isoform, which consequently lacks significant phosphatase activity in the presence of IMP. T2 relaxation NMR and SAXS together support the hypothesis that IMP binding to PMM1 favors an enzyme conformation that is catalytically competent for water attack at the phosphoaspartyl intermediate. Such a mechanism may be generalizable to other enzymes that act through covalent intermediates.

Grapgical Abstract

Address correspondence to: Karen N. Allen, Department of Chemistry, Boston University, 590 Commonwealth Ave., Boston, MA 02215 Tel. 617-358-5544; Fax. 617-358-5554; drkallen@bu.edu.

The coordinates and structure factors of *H. sapiens* PMM1 complexed with IMP, and site-directed variant structures containing mutations R183I, M186Q, R180T/R183I, and R180K/R83K have been submitted to the PDB with accession codes 6CFV, 6CFR, 6CFS, 6CFT, and 6CFU, respectively.

Supporting information. Supplementary Table S1 of crystallographic data collection and refinement statistics, five supplementary figures

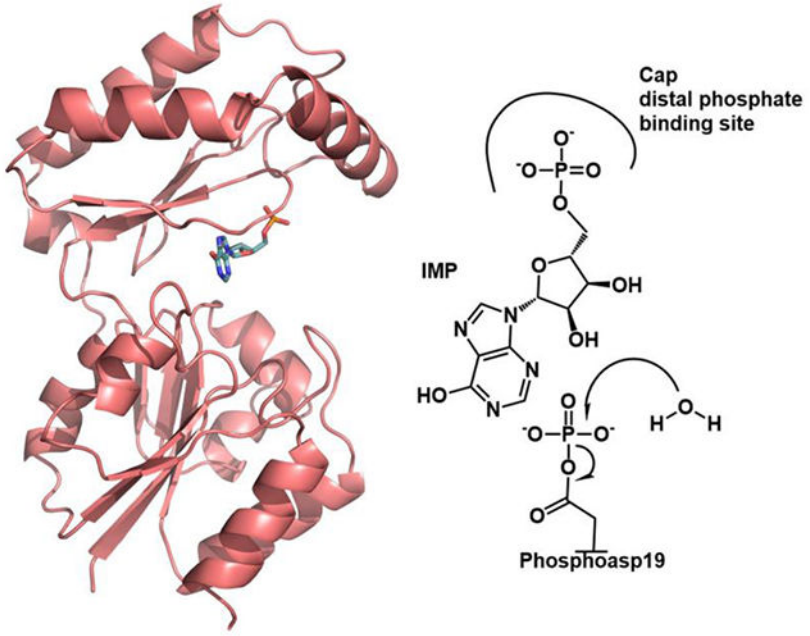

Introduction

Phosphomannomutase (PMM) is a ubiquitously expressed enzyme found in bacteria, plants and animals and is essential in mannose metabolism. In humans, there are two isoforms of phosphomannomutase, which share 66% amino acid sequence identity and 85% similarity. Both PMM1 and PMM2 have comparable k_{cat}/K_m *in vitro* for catalyzing the interconversion of α-mannose 1-phosphate (Man-1-P) to mannose 6-phosphate (Man-6-P) (~10^5 $M^{-1}s^{-1}$).[1,2] Additionally, neither PMM1 nor PMM2 discriminate between monophosphorylated mannose and monophosphorylated glucose substrates as both enzymes also catalyze the interconversion of α-glucose 1-phosphate and glucose 6-phosphate with $k_{cat}/K_m \approx 10^5$ $M^{-1}s^{-1}$.[2] However, despite these similarities, PMM1 and PMM2 have evolved to take on different *in vivo* functions.

Human PMM2 supplies the cell with Man-1-P, an intermediate essential to the N-linked polysaccharide synthesis pathway.[3] This serves as the precursor to GDP-mannose, from which the mannose moiety is transferred to the growing oligosaccharide chain in the endoplasmic reticulum during post-translational protein glycosylation.[4] Deficiencies in PMM2 are associated with a rare inborn error in metabolism – congenital disorder of glycosylation type-1a (CDG-1a).[5–7] CDG-1a patients experience varying severity of nervous system defects with symptoms including cognitive impairment, speech difficulties, psychomotor retardation, developmental delay, vision problems, seizures and stroke-like episodes.[7–9] Conversely, PMM1 has not been shown to be associated with disease, and PMM1 gene knockout in mice exhibited no abnormal phenotype.[10] Due to the sequence, functional and structural similarity between the two isoforms, the activity of PMM1 and its capacity to compensate for a loss of PMM2 activity[10,11] has been analyzed. Thus far, there has been no evidence to show that PMM1 can compensate for deficiencies in PMM2.[10] This

lack of complementarity may be due, *in vivo*, to the differential tissue expression of PMM1 and PMM2. PMM2 is expressed in all tissues, whereas PMM1 is expressed primarily in the brain with lower expression in lung, heart and kidney of human and rat tissues.[3,12,13] To date, the function of PMM1 remains unclear.

In 2008, the group of Van Schaftingen showed that PMM1 may play a role in glycolytic rescue during a temporary shortage of blood to the brain.[1] They identified PMM1 as the inosine monophosphate (IMP) activated glucose 1,6-bisphosphate (Glu-1,6-P_2) phosphatase in the brain that was first described by Guha and Rose.[1,14,15] The Glu-1,6-P_2 phosphatase-catalyzed reaction is seen to occur under ischemic conditions in the brain where ATP depletion leads to an increase in its metabolic product, IMP, through the action of adenosine deaminase on ADP. Notably, even under saturating IMP conditions, PMM2 shows no significant phosphohydrolase activity *in vitro*.[1]

Glu-1,6-P_2 is biosynthesized from glycerate-1,3-P_2 as the phosphoryl donor and α-glucose 1-phosphate (Glu-1-P) or Glu-6-P as acceptor.[16,17] The brain and red blood cells contain the highest concentration of Glu-1,6-P_2 at ~70-80 μM; however, this supply is rapidly metabolized during ischemic conditions.[18] Additionally, during brain ischemia, a shortage of oxygen and glucose to the brain causes depletion of ATP, thus, elevating the concentration of ATP metabolites, including IMP. Basal level concentrations of cellular IMP range from 0.02-0.3 mM and 3-10 mM for ATP. Under hypoxic or ischemic conditions, IMP concentrations are elevated to 0.2-0.6 mM and ATP decreases to 1-5 mM, as measured in rat/pigeon heart.[19–21] In the brain, excess Glu-1,6-P_2 serves as a reserve to temporarily maintain glycolysis via PMM1 phosphatase activity. As the IMP concentration increases, PMM1-catalyzed phosphatase activity is activated, catalyzing hydrolysis of Glu-1,6-P_2 to produce inorganic phosphate and Glu-6-P. This product then enters into the second glycolytic step – the conversion of Glu-6-P to fructose 6-phosphate (Fru-6-P) by phosphoglucose isomerase (Figure 1). Notably, Glc-1,6-P_2 is an inhibitor of brain hexokinase, thus, decreasing the concentration of Glu-1,6-P_2 increases hexokinase activity. As ischemia progresses, increased levels of IMP activate glycogen phosphorylase.[15]

PMM1 and PMM2 are members of the haloalkanoate dehalogenase superfamily (HADSF). HADSF members are structurally comprised of a core Rossmann fold housing four conserved sequence motifs that confer phosphoryl-group and Mg^{2+} cofactor binding and catalytic activity.[22] Motif 1 contains the catalytic Asp residues with a conserved Asp_nXAsp_{n+2} sequence, wherein Asp_n acts as the catalytic nucleophile and Asp_{n+2} acts as the general acid-base. Motif 2 and motif 3 together contribute to the binding of the phosphoryl moiety in the enzyme-substrate complex and the phospho-aspartate intermediate[23–26] and to the stability of the transition state.[27] Motif 4 contains conserved acid residue(s) necessary to coordinate the Mg^{2+} cofactor, either directly or through water.[28] The PMM isozymes have a separate “cap” domain inserted between motifs 2 and 3 comprised of four α-helices and a four stranded anti-parallel β-sheet, allowing classification of PMM to the type C2b subfamily of the HADSF. In HADSF members, the cap movement relative to the core results in open and closed forms via a substrate-mediated induced-fit model.[29–31] Unliganded structures of human PMM1 (PDB 2FUC) and human PMM2 (PDB 2AMY) have been determined in an open conformation[2,32] and shown to have nearly

identical architecture with an rmsd of 0.65 Å for the cap and 1.56 Å for the core domains. Additionally, the structure of PMM1 bound to substrate, Man-1-P (PDB 2FUE), was previously determined in the open conformation giving insight to the mutase mechanism of action (Figure 2).[2]

The mechanism of the mutase function of PMM1 and PMM2 has been proposed by Silvaggi *et al.*[2] The PMM phosphoryl transfer mechanism is a two-step reaction with a bisphosphorylated sugar intermediate as observed in the functionally related enzyme from the HADSF, β-phosphoglucomutase (β-PGM). [31, 32] Activation of the enzyme requires the attack of the catalytic aspartyl nucleophile (Asp19 in PMM1 and Asp12 in PMM2) at the phosphoryl group of the bisphosphorylated sugar, Glu-1,6-P_2, forming an aspartylphosphate residue (shown for PMM1 in Figure 3). Subsequently, the substrate Man-6-P (or alternatively Glu-6-P) is recruited by binding to the cap domain and is guided to the active site by the closing of the cap relative to the core. In this solvent excluded, closed conformation, Man-6-P or Glu-6-P is positioned such that the C1 hydroxyl group is adjacent to the aspartylphosphate group and aligned for nucleophilic attack on phosphorus (Figure 3). Thus, the phosphoryl group is transferred to the substrate, and the bisphosphorylated-sugar is then released from the enzyme. Reorientation/flipping of the bisphosphorylated sugar allows the C6 phosphate to be removed by the Asp nucleophile, regenerating the phosphorylated enzyme and releasing the product, Man-1-P.[34] The phosphoryl transfer chemistry is facilitated by the Asp_{n+2} residue, which acts as a general acid/base to deprotonate/protonate the sugar hydroxyl nucleophile/leaving group.[35]

Herein, we report the X-ray crystallographic structure of Mg^{2+} bound PMM1 in complex with IMP. IMP was found to share the identical binding site previously revealed in the crystal structure of human PMM1 bound to the substrate, mannose-1-phosphate (2FUE).[2] Site-directed mutagenesis and kinetic analysis identified key residues that allowed for IMP binding in PMM1, but not in PMM2. SAXS and T2 relaxation NMR studies are consistent with IMP binding favoring a conformer that is catalytically competent for the attack of water on the phosphoenzyme. From these findings, we propose a mechanism for IMP-mediated activation of the phosphatase versus mutase functions in PMM1 and a structural explanation for the differential activity of PMM2 under the same conditions. Additionally, we posit that the activity of other enzymes that act through covalent intermediates may be modulated in a similar fashion.

Materials and Method

Enzymes, plasmids, and reagents

Except where otherwise indicated, all chemicals were obtained from Sigma-Aldrich. Primers, T4 DNA ligase, restriction enzymes, and expression vectors were purchased from Invitrogen. QuikChange II for site-directed mutagenesis was purchased from Agilent. The QIAprep Spin Miniprep Kit was from Qiagen. Host cells, DH5α and SoluBL21, were purchased from NEB and Genlantis, respectively. The BioMol Green™ phosphate assay kit was purchased from Enzo Life Sciences. The α-PMM1 and α-PMM2 were subcloned from commercially available cDNA.

Cloning, Expression, and Purification

The sequences encoding α-PMM1 and α-PMM2 were subcloned from pET-28b(+) or pET-23b(+) vectors described previously[2] into pET-SUMO vectors to yield constructs containing an N-terminus 6x-His epitope and SUMO fusion protein. Both plasmids were transformed into *E. coli* DH5α competent cells for storage. PMM1 variants (R180T, R183I, M186Q, R180T/R183I) and the PMM2 variant (T171R/I174R) were generated using Agilent's QuikChange II kit. The purified plasmids were sequenced by Genewiz.

Recombinant α-PMM1 was purified from *E. coli* SoluBL21 cells cotransformed with the pET-SUMO_α-PMM1 plasmid and pRARE plasmid (encodes tRNA for rare codons in *E. coli*). Transformed cells were grown at 37 °C in Luria broth containing 50 μg/ml kanamycin and 35 μg/ml chloramphenicol and when cells reached an OD600 ~0.6-0.8, were induced for 4 h with 1 mM isopropyl β-D-thiogalactopyranoside (IPTG). Cells were harvested by centrifugation and the pellet was suspended in 100 mL of ice-cold lysis buffer (buffer A: 50 mM Tris pH 8.2, 500 mM NaCl, 5 mM $MgCl_2$, 5 mM DTT, 10 mM imidazole) and lysed by high-pressure mircrofluidizer. Following high-speed centrifugation of lysate, supernatant was loaded onto a GE 5 mL HisTrap HP Ni^{2+} column, and SUMO_α-PMM1 was eluted by a step-wise increase of imidazole concentration between buffer A and B using FPLC (buffer B: 50 mM Tris pH 8.2, 500 mM NaCl, 5 mM $MgCl_2$, 5 mM DTT, 500 mM imidazole). The N-terminal SUMO protein was cleaved by incubation with SUMO protease[36] at 4 °C for 4 h. Separation of PMM1 and SUMO was performed by size-exclusion chromatography using GE Sephacryl S-100 HR. Purified PMM1 was dialyzed in 50 mM Hepes pH 7.2, 5 mM $MgCl_2$ and 1 mM DTT for storage, or 10 mM Hepes pH 7.5, 100 mM NaCl, 5 mM $MgCl_2$ for crystallization. The final yield was ~20 mg protein/g wet cell paste. Expression and purification of α-PMM1 variants and α-PMM2 followed the same protocol and gave similar yields.

PMM steady-state kinetics:

Kinetic assays measuring α-PMM1 phosphoglucomutase activity were carried out at 25 °C in 50 mM Na^+ Hepes, pH 6.5, 10 mM $MgCl_2$. The initial rate at which α-PMM1 catalyzed the conversion of α-Glu-1-P to Glu-6-P was measured by a coupled reaction containing Glu-6-P dehydrogenase and reduction of $NADP^+$ was monitored by the increase in absorbance at λ = 340 nm ($\Delta\epsilon$ = 6.2 mM^{-1} cm^{-1}). Assays were performed in 1-mL quartz cuvette containing 50 μM α-Glu-1,6-P_2, 0.2 mM $NAPD^+$, 5 units/mL Glu-6-P dehydrogenase. The k_{cat} and K_m values were determined by fitting to the Michaelis-Menten equation using the program GraphPad Prism,

$$v_0 = V_m[S]/(K_m + [S]) \quad (1)$$

where [S] is the α-Glu-1-P concentration, v_0 is the initial velocity, V_m is the maximum velocity, and K_m is the Michaelis constant. The k_{cat} was calculated from the ratio of V_{max} and the α-PMM concentration.

The phosphoglucomutase inhibition constant by IMP was determined by the equation

$$V^{app}_{max} = V_{max}/(1 + [I]/K_i) \quad (2)$$

where [I] is the concentration of IMP, and K_i is the inhibition constant. Inhibition assays were performed at a fixed substrate concentration ($5K_m$ α-Glu-1-P) under conditions similar to the coupled assay described above with the exception of the coactivator, Glu-1,6-P_2. In place of α-Glu-1,6-P_2, 2.5 mM fructose 1,6-(bis)phosphate (Fru-1,6-P_2) was used to activate the enzyme (K_{act} of PMM2 by Fru-1,6-P_2 is 480 μM.[34])

The rate of PMM1 phosphatase activity (α-Glu-1,6-P_2 to Glu-6-P and P_i) was assayed using the colorimetric quantitation of phosphate with BioMol Green™ Reagent from Enzo, a molybdate/malachite green-based reagent to simultaneously quench the reaction and begin color development. Absorbance at λ = 620 nm was measured in 96-well plates using a SpectraMax M5 microtiter plate reader (Molecular Devices, Sunnyvale, CA) and quantitation of phosphate hydrolysis was calculated from a phosphate standard curve. The assay was prepared with 0.1 mM IMP in a buffer solution containing 100 mM Hepes, pH 7.2, 2 mM $MgCl_2$, and 2 mM β-mercaptoethanol. Initial velocity was determined by quenching 50 μL of reaction into 100 μL BioMol Green™ reagent in 15 second intervals from time point 0 to 5 minutes, performed in triplicate. The k_{cat} and K_m constants were determined using equation 1. The activation constant by IMP, K_{act}^{IMP}, was determined by varying concentration of IMP (0 – 50 μM for wild-type PMM1), and fitting to the equation

$$v_0 = V_m[A]/(K_{act}^{IMP} + [A]) \quad (3)$$

where [A] is the concentration of IMP.

Crystallization and X-ray crystallographic data collection:

PMM1 crystals were grown in 20% polyethylene glycol 3350, 0.15 M DL-malate, pH 7.0, 50 mM $MgCl_2$, and 8 mM β-mercaptoethanol by the hanging-drop vapor diffusion method.[2] Drops were formed by mixing 1 μL of well solution with 1 μL of 15 mg/mL purified protein in 10 mM Hepes pH 7.5, 100 mM NaCl, and 5 mM $MgCl_2$. Diffraction quality crystals formed after two rounds of micro-seeding in 2 days at 17 °C. Crystals of PMM1 complexed with IMP were obtained by soaking in a solution of 10 mM Hepes pH 7.5, 100 mM NaCl, 5 mM $MgCl_2$ with 200 mM IMP for 6 hours prior to flash-cooling. Crystals were transferred to Paratone-N and flashed-cooled in liquid N_2. X-ray diffraction data was collected via remote access to Stanford Synchrotron Radiation Lightsource (SSRL) Beamline 12-2. PMM1 in complex with IMP crystallized in space group $P4_32_12$ with unit cell dimensions a = b = 52.17 Å, c = 214.48 Å. Crystal size was 0.7 x 0.3 x 0.3 mm^3 and crystals diffracted to 1.92 Å resolution. The data set was indexed, integrated and scaled in autoXDS.[37]

Crystals of PMM1 variants M186Q, R183I, R180K/R183K grew in the same condition as wild-type PMM1. Crystals of variant R180T/R183I were grown in the same condition with the addition of 0.05 M L-lysine. Although there is no density for L-lysine in the structure, the presence of the positively charged amino acid appears to improve crystal formation. The R180T variant did not yield crystals. Data sets for R180T/R183I and R180K/

R183K were collected at the National Synchrotron Light Source (NSLS) at Brookhaven National Laboratory (BNL) on beamline X-25, and the data sets for R183I and M186Q were collected at the Advanced Photon Source (APS) at Argonne National Laboratory (ANL) on beamline 24-ID-E. See supplementary information Table S1 for crystallographic data collection statistics for PMM1 variants.

Structure Determination and Model Refinement:

The structure of PMM1 in complex with IMP was determined using phases calculated by molecular replacement using the wild-type PMM1 structure (PDB 2FUC) as the model. An initial model was built using Phenix AutoBuild[38] and improved by manual rebuilding in the molecular graphics suite COOT.[39] The model was refined in PHENIX Refine.[38] After rigid body refinement in PHENIX Refine (at R_{work} = 0.19), the electron density for inosine-monophosphate (IMP) was well defined and the ligand was added to the model. Iterative cycles of restrained refinement in PHENIX Refine and rebuilding in COOT ultimately yielded a model containing 240 of 262 residues, 307 water molecules, and 2 Mg^{2+} ions. The quality of the model was assessed by MOLPROBITY,[40] and a Ramachandran plot showed 235 residues (96.7%) were in the favored regions, 7 residues were in the additionally allowed regions, and no residues were in the disallowed regions. Data collection and refinement statistics for PMM1-IMP models are reported in Table 1. Structures of PMM1 variants were determined and refined in the same manner. (See supplemental Table S1 for model refinement statistics of PMM1 variant structures).

PMM SAXS and WAXS data:

SAXS experiments were performed at beamline X9A at NSLS, at a wavelength of 0.918 Å and beam energy of 13.5 keV. Data were initially collected at varying concentrations of protein (1.25 – 28 mg/mL) to determine optimal concentrations and examine concentration-dependent changes. The scattering curve and radius of gyration (R_g) did not change within the tested concentration range indicating stable oligomer formation in solution (data not shown). Consequently, all other data were collected at a constant protein concentration of 10 mg/mL in a buffer solution containing 50 mM HEPES, 100 mM NaCl, 5 mM $MgCl_2$, 1 mM β-mercaptoethanol (βME) at pH 7.5 and ligands at a concentration of 10 mM at 14 °C. The sample-to-detector distance for SAXS data collected on a MarcCCD 165 was 3.4 m and WAXS data were collected simultaneously at 0.47 m from the sample. The sample-to-detector distance resulted in a resolution range of $0.0064 < q = 4\pi/\lambda < 2.0$, where $q = 4\pi \sin\theta/\lambda$ and 2θ is the scattering angle. For data collection, a 20 μL sample volume was continuously loaded in a 1 mm diameter capillary and exposed to X-rays for 30 s. Each sample was collected in triplicate and averaged. The buffer component of the scattering was removed by subtracting the scattering data from dialysate of the sample to produce the 1D scattering curve of the macromolecule. The scattering intensity normalization and Guinier approximation calculations were carried out in Primus of the ATSAS suite.[41] The R_g was determined using Guinier analysis of low resolution data by the Guinier approximation,

$$I(q) = I(0) \exp(-q^2 R_g^2/3) \quad (4)$$

with a qRg limit of 1.3, which is within the standard guideline of qRg to signify a valid Guinier approximation. The molecular envelope of PMM1 complexed with IMP was generated by *ab initio* shape reconstruction in DAMMIN.[42] The reconstructions generated with no symmetry (P1) or with P2 symmetry enforced were virtually indistinguishable.

T_2 Relaxation NMR:

NMR spectra were collected at Boston University Medical Campus on a Bruker DMX 500. Purified protein was prepared to a final concentration of 50 μM with saturating ligand concentration of 0.9 mM IMP in storage buffer (50 mM Hepes pH 7.2, 5 mM $MgCl_2$ and 1 mM DTT) and transferred to 5 mm NMR tubes (Wilmad laboratory glass). NMR spectra were acquired with 16 scans and a recycle delay of 1 s. Typical 90° and 180° pulse lengths of 10 and 20 μs, respectively, were used according to published procedures.[43]

Results

Overall structure

In order to assess the structural basis for the IMP-triggered switch between phosphatase and mutase activity, the structure of PMM1 in complex with IMP was determined to 1.93 Å resolution (Figure 4A and B, see Table 1 for data collection and refinement statistics). The IMP-liganded protein crystallized under the same conditions as those previously used for the unliganded enzyme[2] and in the same unit cell and space group. Similar to the native PMM1 structure, the first eleven residues of the N-terminus and the last six residues of the C-terminus were disordered; the electron density for the remainder of the protein was clear and ordered. PMM1 is comprised of a 100 amino-acid long C2b type cap domain (residues 95-194 of PMM1) containing α-helices and β-sheets in a αααββαββ orientation inserted between β5 and α7 (or motifs 2 and 3) of the Rossmann-fold core domain. The core domain (residues 1-90 and 198-262) Rossmann fold comprises 6 parallel β-sheets (β1-β5 and β10-β11) encircled by 5 α-helices (α1-α2 and α7-α9). The cap and core are connected by two solvated hinge regions composed of residues 91-94 and 195-197 (Supplemental Figure S1). The biological assembly of PMM1 is a dimer joined together exclusively by intermolecular interactions at the α4 helix and β6 strand of the cap region; the dimer was previously verified as the oligomeric species in solution via size-filtration chromatography.[2] However, as the binding sites are catalytically independent (no cooperativity or half-sites reactivity), the figures and descriptions herein will be in the context of a single subunit unless otherwise stated.

In all crystal forms known, human PMM1 assumes the cap open conformer; as this structure was obtained by soaking crystals of PMM1 with IMP, the crystal lattice would prevent the domain motions required to close the active site. As is seen for the mode of binding of Man-1-P,[2] the activator IMP is bound via interactions with the cap domain and does not make interactions with the core domain phosphoryl-transfer site. A superposition between the structure of the PMM1/IMP complex with those of the unbound form of PMM1 (PDB 2FUC) and PMM1 in complex with Man-1-P (PDB 2FUE) shows that the IMP-bound structure differs minimally from the other two with rmsd of 0.37 Å and 0.55 Å, respectively (Figure 5). [Notably, the rmsd is somewhat biased as the phases for PMM/IMP structure

were determined by molecular replacement with the 2FUC coordinates.] The core domain structures do not differ significantly, and the cap domain varies little with the exception of the substrate-binding loop. In the IMP bound enzyme, there is less β-strand structure and a more extensive loop region extending from residues 181-189 due to the disruption of hydrogen bonds from β8-strand to β9-strand of the β sheet of the cap domain (Figure 5A, top right). Presumably, these changes are caused by the binding of IMP. The presence of Man-1-P in the substrate-bound structure also increases the amount of loop structure in the cap, however, to a lesser degree than for IMP (Figure 5A, bottom right). Notably, the resulting loop structure (residues 179-189) is not disordered, as indicated by the fact that the B-factors for unliganded, Man-1-P bound and IMP bound PMM1 structures in the loop are similar to the average B-factor for the protein. We propose that the β8 strand and the connecting loop between β8 and β9, residues 179-189, provide the binding determinants for IMP and are thus critical for modulating PMM1 phosphohydrolase versus mutase functionality.

IMP binding to the substrate distal phosphoryl-group binding site suggests competitive binding

The structure of PMM1 in complex with IMP reveals IMP bound at the cap domain, sharing the same binding site as substrate Man-1-P (PDB 2FUE). Thus, there is no separate allosteric site on PMM1 responsible for IMP-activated phosphohydrolase activity. Previous structural and mutational analyses of HADSF enzymes in general, and specifically of PMM1, have demonstrated that the cap domain is responsible for substrate binding and discrimination.[2,44–48] The substrate phosphoryl binding site in the cap domain is termed the distal phosphate binding site (as it is distinct from the transferring binding site in the core domain where chemistry occurs). The side chains that make hydrogen bonds with the substrate phosphate moiety of Man-1-P in the distal site include Arg143, Arg150, Ser188, and the amide backbone of Met186[2] (Figure 5B). In the PMM1-IMP complex, the phosphoryl moiety of IMP binds at the same site as the phosphoryl moiety Man-1-P, namely the distal binding site. Moreover, in the course of the IMP associated phosphatase activity, product analysis by HPLC shows that IMP does not become phosphorylated (data not shown). These findings are consistent with a model in which IMP binding activates the transfer of the phosphoryl group to water (Figure 3) doing so, in part, by blocking the binding of the phosphohexose sugar.

In addition to those residues that interact with Man-1-P, the inosine moiety forms hydrogen bonds with the amide backbone of Gly184 and the side chains of Ser182, Asp190, Asn137, and Arg132 (Figure 5C). Notably, although IMP does not bind to PMM2,[1] these same residues are conserved in that isozyme with the exception of Met186, which occurs as Gln177 in PMM2. Thus, additional binding determinants must be present in PMM1.

Sequence alignment of PMM homologs identifies differential conservation of residues between PMM1 and PMM2 in the IMP binding-loop region

Because residues that interact through hydrogen bonds to the effector IMP are conserved in both PMM1 and PMM2, differences in sequence between PMM1 and PMM2 surrounding the binding site were sought out. The analysis was focused on the sequences comprising

β8 and the extended loop involved in ligand binding. This region is highly conserved with three striking differences – Arg180, Arg183, and Met186 in PMM1 occur as Thr171, Ile174, and Gln177 in PMM2, respectively. Furthermore, examination of iso-functional orthologs of PMM1 and PMM2 showed these differences were conserved (Figure 6). It is possible that the positively charged residues play a role in IMP binding, and the Thr171 and Ile174 side chains in PMM2 might contribute to the stability of the β-strand and prohibit the flexibility required to accommodate a purine nucleotide (Figure 7a). To test this hypothesis, five site-directed variants of PMM1 and one of PMM2 were generated, and the role of each residue was assessed by testing the enzyme variants for IMP binding and for phosphatase activity. Single-site mutations of PMM1 were made to replace the charged arginines and methionine with the corresponding PMM2 side chains – R180T, R183I, and M186Q. Two double mutations were generated – R180T/R183I to assess the additive effect of replacing both arginine residues with the PMM2 counterparts and R180K/R183K to test if the positive charge is key to IMP binding. Finally, T171R/I174R mutations were generated in PMM2 to test whether these two residues were sufficient for IMP binding. For each variant, the kinetic constants were first determined for mutase activity to confirm that the protein was properly folded and active (Table 2). The k_{cat} and K_m for mutase activity of all PMM1 variants do not differ significantly from those of wild-type PMM1 (~0.5-1.5 fold difference in k_{cat} and ~0.5–2.5 fold difference in K_m). Steady-state kinetic constants for PMM2 were also determined to confirm and compare to the previously reported values.[2] Notably, the T171R/I174R PMM2 variant failed to yield any detectable mutase activity nor did it acquire phosphatase activity. Overall, the unchanged steady-state kinetic constants show that the PMM1 variants retained their native fold and that substrate-binding and mutase activity has not been affected by the replacement of these amino acids.

Phosphatase activity in the presence and absence of IMP was measured for each construct (Table 3). For wild-type PMM1, phosphatase activity increased by two orders of magnitude in k_{cat}/K_m in the presence of saturating IMP (100 μM), reflecting an increase in the turnover rate (k_{cat}) without a significant change in K_m. In the absence of IMP, k_{cat} for Glu-1,6-P_2 hydrolysis was 0.018 s^{-1} and increased by 78-fold to 1.4 s^{-1} in the presence of 100 μM IMP. This rate of hydrolysis in the absence of IMP is slow, but significant, such that the phosphenzyme is not considered to be kinetically stable. All single PMM1 variants, R180T, R183I, and M186Q, exhibited similar k_{cat} and K_m values for phosphatase activity compared to wild-type in the presence and absence of IMP. However, the phosphatase activation constant, K_{act}^{IMP}, differed drastically. The IMP concentration required for half the maximum phosphatase activity increased by 120-fold for R183I, 9-fold for R180T and 5-fold for M186Q. These fold increases are in agreement with the IMP inhibition constants, K_i^{IMP}, determined for PMM1 mutase activity (Table 2). The K_i^{IMP} of 2.0 μM for wild-type PMM1 mutase activity is similar to the phosphatase K_{act}^{IMP}, at 1.5 μM. The same trend is observed in the PMM1 variants where the R183I variant was most detrimental to mutase inhibition by IMP, increasing the K_i^{IMP} to 350 μM compared to wild type, a 175-fold increase. PMM1 variants R180T and M186Q exhibited minimal change in K_i^{IMP} compared to wild-type, where K_i^{IMP} are 2.3 μM and 2.8 μM, respectively. Overall, the roles of R180, R183 and R180T appear to be in IMP binding rather than in catalysis of phosphoryl transfer

to water, as wild-type k_{cat} rates of phosphohydrolase activity can be achieved with saturating activator levels.

Next, we tested whether there were synergistic effects from mutating both arginine residues in PMM1 to the corresponding PMM2 residues by constructing R180T/R183I. Phosphatase activity in the R180T/R183I variant reflected a significant loss of IMP-dependent activation. In the absence of IMP the phosphohydrolase activity was relatively unchanged compared to wild type (the same k_{cat} with only a 3-fold increase in K_m). Notable, however, at saturating IMP concentration (2 mM IMP), k_{cat} decreased 9-fold and K_{act}^{IMP} increased by over 500-fold. Because phosphatase activity is changed to a small extent, but large amounts of IMP are required for activation, we posit that positive electrostatics around the cap-core interface play an important role in IMP binding (Figure 7b). To test this hypothesis, we made a second double variant to replace the arginine residues by positively charged residues, R180K/R183K. Consistent with our prediction, k_{cat}, K_m, and K_{act}^{IMP} remained comparable to wild-type with a high binding affinity for IMP (Table 3). In both double PMM1 variants, the K_i^{IMP} of the mutase activity were in agreement with K_{act}^{IMP} of the phosphatase activity. Whereas in the R180T/R183I variant K_i^{IMP} and K_{act}^{IMP} increased by 390-fold and 560-fold, respectively, the inhibition and activation constants for the R180K/R183K variant remained relatively unchanged compared to those of wild type (see Supplemental Figures S2 and S3 for kinetic data). X-ray crystallographic structures of the PMM1 variants R183I, M186Q, R180T/R183I, R180K/R183K were determined showing no significant changes from the structure of wild-type PMM1 (see Supplemental Table 1 for crystallographic statistics). PMM1 variant R180T did not yield crystals.

Additionally, the PMM2 variant containing the double mutation T171R/I174R was made to test if a gain of function could be achieved, in which PMM2, like PMM1, would bind IMP and allow for Glu-1,6-P_2 hydrolysis. Unfortunately, this variant was inactive for mutase and phosphatase activity, although purification, gel filtration and SAXS experiments showed that the majority of protein was soluble and folded.

NMR T2 relaxation experiments

T2 relaxation time measurement of small molecules by NMR was used for ligand-protein interaction measurements by exploiting the change in relaxation rate of a small molecule when bound to a protein molecule. The relaxation time of the ligand alone was compared to that of the ligand in presence of the protein. A total of five samples were measured, including free IMP ligand and four samples of protein-ligand mixtures. Relative signal intensity was plotted as a function of relaxation time (s) delay at which signal intensity is measured (Figure 8). At 0.32 s, the free ligand ^{1}H NMR signal intensities were reduced by 30%, whereas in the mixture of IMP with wild-type PMM1 (with an affinity of 2 μM) signal intensities were reduced by 70%. As expected, the sample containing IMP and the R180T/R183I variant exhibited a nearly identical relaxation curve to that of the free ligand curve, demonstrating little to no ligand interactions with this variant. Surprisingly, solutions containing IMP with wild-type PMM2 resulted in a 40% signal reduction at 0.32 s – a 10% increase in relaxation time. This demonstrates that IMP was interacting with PMM2, but the interaction was much weaker in PMM2 as compared to PMM1. Furthermore, the T171R/

I174R PMM2 variant (which is a catalytically inactive enzyme) exhibited a faster relaxation rate compared to that of free ligand. For T171R/I174R at 0.32 s, the signal was reduced by 43%, and at 0.64 s the signal was reduced by 70%. The values are similar between active wild-type PMM2 (active for mutase activity) and the inactive T171R/I174R PMM2 variant; thus, in PMM2, the mode of IMP interaction leading to increase in T2 relaxation rate compared to free IMP is not one that is associated with phosphatase activity. Taken together, the data show that IMP binds most efficiently to wild-type PMM1 and that R180 and R183 are necessary for IMP binding in PMM1. Wild-type PMM2 and the T171R/I174R PMM2 variant exhibited IMP binding, but neither protein catalyzes phosphatase activity. These results support the hypothesis that in the case of wild-type PMM2 and variant PMM2, IMP is capable of binding the protein, but it does not produce the catalytically competent complex for phosphohydrolase activity.

Conformational changes in PMM1 and PMM2 induced by ligand binding

SAXS experiments were performed to analyze the interdomain motions of cap and core domains in PMM1 and PMM2 upon ligand binding. A range of protein concentrations (1.25 mg/mL to 28 mg/mL) were first measured for PMM1 without ligand to assess the concentration dependence of the observed conformation and potential of dimerization (PMM1 and PMM2 are dimeric[2]). The Guinier plot showed acceptable linearity in the low-resolution scattering range for determination of the radius of gyration (R_g) (Figure S4). At all concentrations, the R_g remained relatively unchanged (R_g = 33.5 ± 0.21 Å), consistent with a stable dimeric state independent of concentration (Figure 9). Unliganded PMM2 at 10 mg/mL had an R_g of 28.1 ± 0.14 Å. The calculated molecular envelope of PMM2 superimposes well with the unliganded crystallographic structure (PDB 2AMY) confirming that the dimer interface between the cap domains observed in the crystal structure exists in solution (Figure S5). It should be noted that whereas PMM2 and R180T/R183I PMM1 produced ideal SAXS scattering curves, wild-type PMM1 consistently showed limited aggregation. However, the R_g in each experiment is highly reproducible, which leads us to believe that the changes observed in the R_g with and without ligand is a true reflection of ligand-induced conformation change.

The effects of ligand binding on the conformation of PMM were examined. In a theoretical scattering curve generated from X-ray crystal structures in FoXS,[49,50] the “open” unliganded PMM1 from *Leishmania mexicana* (PDB 2I54)[51] dimer had R_g = 27.2 Å, and the “closed” PMM1 conformation bound to Glu-1,6-P_2 (PDB 2I55) had R_g = 24.4 Å – predicting a ~2.8 Å difference in R_g between the conformers (Figure 9). In a comparison between wild-type PMM1, PMM2 and the R180T/R183I PMM1 variant, we observed smaller radii of gyration when PMM was bound to ligands that mimic the transition state (e.g. VO_4^{3-} or VO_4^{3-}/Glu-1-P) compared to the unliganded state. These differences in R_g between the open and closed forms of PMM1 are comparable in magnitude (percent change) to those calculated from the X-ray crystal structures of the *L. mexicana* PMM1 in the open and closed forms. The R_g was reduced in all cases where VO_4^{3-} is present, suggesting that VO_4^{3-} is sufficient to induce a closed conformation. It should be pointed out that VO_4^{3-} alone acts as a phosphoenzyme-intermediate analogue and may also simultaneously bind to the leaving-group binding site (the non-transferring phosphate binding site) on the

cap mimicking the phosphoryl moiety of substrate Glu-1-P or Glu-6-P; thus for PMM2, VO_4^{3-} alone yields similar R_g values to those for transition-state analogs VO_4^{3-}/Glu-1-P and VO_4^{3-}/Glu-6-P. Compared to this VO_4^{3-} complex, smaller R_g values were obtained when PMM1 was bound to a transition-state analog, i.e. VO_4^{3-}/Glu-1-P and VO_4^{3-}/Glu-6-P (Figure 9). Notably, in PMM1 the VO_4^{3-}/IMP complex resulted in R_g values similar to those of the transition-state analog complexes. The R180T/R183I PMM1 variant and wild-type PMM2 showed similar trends to one another with the addition of ligands. Moreover, based on the change in R_g, IMP binding alone is sufficient to induce a conformational change in wild-type PMM1 (compared to unliganded) but appears to have minimal effect on the R180T/R183I PMM1 variant or wild-type PMM2. The presence of IMP resulted in a mere 0.1 Å and 0.6 Å difference in the R_g of R180T/R183I PMM1 and PMM2, respectively, suggesting that IMP either does not bind or binds but does not induce a closed "catalytically competent" conformation. To confirm that the observed decrease in R_g is a result of ligand binding and not its presence in bulk solution, glucose was used as a negative control. As glucose does not contain a phosphoryl moiety, we expect that the addition of glucose would result in the same conformer ensemble as the unliganded protein. As expected, for wild-type PMM1, the R_g remained unchanged in the presence of glucose compared to the no ligand condition, and R_g was similar in the presence of IMP, or glucose or with no ligand in R180T/R183I PMM1 and PMM2. Together with the results from steady-state kinetics and NMR, the SAXS analysis of PMM1 and PMM2 support the model that IMP binding to PMM1 favors cap closure into a conformation catalytically competent for hydrolysis of the phosphoaspartyl intermediate, whereas IMP binding to PMM2 does not result in adoption of the catalytically competent conformer.

Discussion

Substrate/effector recognition and regulation

Our crystallographic results show that the effector IMP is recognized in a similar manner as substrate. The loop of the cap domain at the cap-core domain interface contains the essential residues responsible for binding of the substrate phosphoryl moiety (the non-transferring phosphate), forming hydrogen bonds to the side chains of Arg143 and Arg150 and to the amide backbone of Met186 and Ser188. The structure of IMP-bound PMM1 shows that these side-chain interactions are also responsible for IMP binding (Figure 5B and 5C). Residues making hydrogen bonds to hydroxyl groups of the mannose moiety include Asp190 and Arg132, and those to the inosine moiety of IMP include Arg132, Asn137, Ser182, Gly184, and Asp190. These side chains are also conserved in PMM2 (with the exception of Met186). Notably, all of the residues involved in IMP binding to PMM1 are conserved in PMM2, yet PMM2 phosphatase activity was not affected by IMP. Via sequence analysis, we have identified three residues, R180, R183 and M186 of PMM1 (T171, I174 and Q177 of PMM2) that differ between human PMM1 and PMM2 within the ligand-binding loop, but are conserved in their respective iso-functional orthologs (Figure 6). Two of the three residues, Arg183 and Met186, also were identified previously as important by computational analysis of the evolutionary divergence between PMM1 and PMM2.[52]

Determination of steady-state rate constants of site-directed variants revealed the key residues affecting IMP binding and the activation of phosphatase activity. A mutation in Arg183 to a hydrophobic isoleucine was the single mutation most detrimental to IMP binding, as measured by the hydrolysis of Glu-1,6-P_2. The measured k_{cat} and K_m for phosphatase activity were comparable to wild-type PMM1, catalyzing the reaction at k_{cat} of 1.4 s^{-1} and K_m of 8.5 μM in wild-type PMM1 and k_{cat} of 1.1 s^{-1} and K_m of 10 μM in R183I. However, the activation constant by IMP increased significantly (120-fold). Introduction of the double mutation, R180T/R183I, resulted in the greatest loss of IMP binding, having a K_{act}^{IMP} 500-fold greater than that of wild-type and a k_{cat} decreased by one order of magnitude (Table 3). Likewise, the inhibition constants, K_i^{IMP}, of mutase activity by IMP in all PMM constructs are comparable to the activation constants (Table 2 and Table 3). These results suggest that the Glu-1,6-P_2 hydrolysis is dependent on the ability of IMP to bind to the enzyme.

Mechanism of phosphatase activity activation and mutase inhibition

Because IMP is bound at the same site as substrate Man-1-P and the SAXS data suggests a conformation change to a more compact particle in the presence of IMP, we hypothesize that PMM1 forms a closed complex, which, in the absence of singly phosphorylated sugar, results in hydrolysis of the phosphoenzyme by water. In this model, IMP binding favors cap closure in the same manner as when bound to substrate or bis-phosphorylated coactivator. But, when the cap domain closes over the core domain in an IMP induced manner, there is no acceptor on IMP for the phosphoryl group. Instead, a water molecule at the active site can accept the phosphoryl group from the phosphoaspartyl moiety. Thus, the coactivator, Glu-1,6-P_2, becomes a substrate because the phosphoaspartate nucleophile is continuously hydrolyzed to produce the unactivated, dephosphorylated form of the enzyme (Figure 10).

Conclusions

IMP binding allows for PMM1 to form the catalytically competent conformer for phosphoryl transfer. However, the metabolite competes with phosphohexose binding, preventing phosphorylated sugar substrates from accessing the active site of the phosphoenzyme and allowing nucleophilic attack by a water molecule, resulting in phosphatase activity. Thus, PMM1 displays a metabolite-dependent enzyme mechanism. The switch between phosphatase and mutase activity is essentially a change in selectivity between a water molecule and a phospho-sugar substrate in the second step of the reaction mechanism. Indeed, selection against water is a common mechanistic problem in phosphotransferases. The manner in which selectivity is brought about by PMM1 and the HADSF mutase β-phosphoglucomutase, through achievement of the catalytically competent conformer rather than by the exclusion of water,[31] is also the case in mechanistically unrelated kinases. In hexokinase, creatine kinase, and ketohexokinase, for example, ligand induced conformational changes allow for the attainment of the competent conformer, preventing ATP hydrolysis.[53–57] In an analogous manner to the effect of IMP on phosphoenzyme hydrolysis in PMM1, the addition of xylose or lyxose (with H in place of the CH_2OH group of glucose) significantly enhances the rate of hexokinase-mediated ATP hydrolysis.[54]

In recent years, many examples of multifunctional enzymes involved in various cellular processes have emerged, with over 6,500 cases gathered from the literature.[58] These multifunctional enzymes include moonlighting enzymes, substrate promiscuous enzymes, or catalytically promiscuous enzymes, in which one gene participates in more than one cellular pathway. It has been speculated that multifunctional enzymes are Nature's way to meet the expanding demands of reactions necessary for higher organisms without the expansion of genetic material.[59] Such novel functions arise unintentionally, but if advantageous, will be selected for and enhanced during evolution.[60] In any case, many enzymes are likely to participate in a secondary function.

The unique secondary function of PMM1 induced by a small molecule metabolite highlights the concept that some enzymes may inherently be evolved to support more than one reaction or cellular purpose. The Glu-1,6-P_2 phosphatase activity of PMM1 does not fall into the category of a moonlighting activity, as the mechanism is the same and the independency of mutase and phosphatase functions is not complete (i.e., mutation of catalytic residues for phosphoryl transfer would inactivate both functions). Rather, the phosphatase activity falls into the category of substrate promiscuity or ambiguity, where the "switch" to turn on and off the alternate reaction pathway is dictated by the cellular availability of the metabolite IMP. Indeed, reactions in which a covalent intermediate of an isomerase or a transferase reaction forms a transient enzyme-substrate complex have the potential to "switch" to a hydrolase reaction in the presence of a metabolite that prevents completion of the latter steps of catalysis. It has been noted that multi-step electron transfer with a covalent enzyme-substrate intermediate step is a prevalent phenomenon in enzyme reactions that allows enzymes to be so proficient.[61] This suggests that in the case of PMM1, enzyme activation of a secondary function by a small metabolite may be a common reaction in nature and opens the possibility that other characterized enzymes may take on a similar "switch" in mechanism.

Supplementary Material

Refer to Web version on PubMed Central for supplementary material.

Acknowledgements.

Financial support for this work was provided by NIH (R01 GM61099 to KNA and DD-M. This work is also based upon research conducted at the Stanford Synchrotron Radiation Lightsource Beamline 12-2, which is supported by the U.S. Department of Energy, Office of Science, Office of Basic Energy Sciences under Contract No. DE-AC02-76SF00515; Brookhaven National Laboratory (BNL) beamline X-25, which is operated for the DOE Office of Science under Contract No. DE-AC02-98CH10886; and at the Northeastern Collaborative Access Team beamlines, which are funded by the National Institute of General Medical Sciences from the National Institutes of Health (P41 GM103403).

References

1. Veiga-da-Cunha M, Vleugels W, Maliekal P, Matthijs G, and Van Schaftingen E (2008) Mammalian phosphomannomutase PMM1 is the brain IMP-sensitive glucose-1,6-bisphosphatase. J. Biol. Chem 283, 33988–33993. [PubMed: 18927083]
2. Silvaggi NR, Zhang C, Lu Z, Dai J, Dunaway-Mariano D, and Allen KN (2006) The X-ray crystal structures of human alpha-phosphomannomutase 1 reveal the structural basis of congenital disorder of glycosylation type 1a. J. Biol. Chem 281, 14918–14926. [PubMed: 16540464]

3. Matthijs G, Schollen E, Pardon E, Veiga-da-Cunha M, Jaeken J, Cassiman J-J, and Van Schaftingen E (1997) Mutations in PMM2, a phosphomannomutase gene on chromosome 16p13, in carbohydrate-deficient glycoprotein type I syndrome (Jaeken syndrome). Nature. 17, 21–24.

4. Kornfeld R, and Kornfeld S (1985) Assembly of asparagine-linked oligosaccharides. Annu. Rev. Biochem 54, 631–664. [PubMed: 3896128]

5. Van Schaftingen E, and Jaeken J (1995) Phosphomannomutase deficiency is a cause of carbohydrate-deficient glycoprotein syndrome type I. FEBS Lett. 377, 318–320. [PubMed: 8549746]

6. Grunewald S (2002) Congenital disorders of glycosylation: A review. Pediatr. Res 52, 618–624. [PubMed: 12409504]

7. Grünewald S (2009) The clinical spectrum of phosphomannomutase 2 deficiency (CDG-Ia). Biochim. Biophys. Acta 1792, 827–834. [PubMed: 19272306]

8. De Lonlay P, Seta N, Barrot S, Chabrol B, Drouin V, Gabriel BM, Journel H, Kretz M, Laurent J, Le Merrer M, Leroy a, Pedespan D, Sarda P, Villeneuve N, Schmitz J, van Schaftingen E, Matthijs G, Jaeken J, Korner C, Munnich a, Saudubray JM, and Cormier-Daire V (2001) A broad spectrum of clinical presentations in congenital disorders of glycosylation I: a series of 26 cases. J. Med. Genet 38, 14–19. [PubMed: 11134235]

9. Marquardt T, and Denecke J (2003) Congenital disorders of glycosylation: review of their molecular bases, clinical presentations and specific therapies. Eur. J. Pediatr 162, 359–379. [PubMed: 12756558]

10. Cromphout K, Vleugels W, Heykants L, Schollen E, Keldermans L, Sciot R, D'Hooge R, De Deyn PP, Von Figura K, Hartmann D, Körner C, and Matthijs G (2006) The normal phenotype of Pmm1-deficient mice suggests that Pmm1 is not essential for normal mouse development. Mol. Cell. Biol 26, 5621–5635. [PubMed: 16847318]

11. Thiel C, Lübke T, Matthijs G, Von Figura K, and Körner C (2006) Targeted disruption of the mouse phosphomannomutase 2 gene causes early embryonic lethality. Mol. Cell. Biol 26, 5615–5620. [PubMed: 16847317]

12. Hansen SH, Frank SR, and Casanova JE (1997) Cloning and characterization of human phosphomannomutase, a mammalian homologue of yeast SEC53. Glycobiology. 7, 829–834. [PubMed: 9376685]

13. Pirard M, Achouri Y, Collet JF, Schollen E, Matthijs G, and Van Schaftingen E (1999) Kinetic properties and tissular distribution of mammalian phosphomannomutase isozymes. Biochem. J 339, 201–207. [PubMed: 10085245]

14. Guha SK, and Rose ZB (1983) Role of inosine 5-phosphate in activating glucose-bisphosphatase. Biochemistry. 22, 1356–1361. [PubMed: 6301545]

15. Guha SK, and Rose ZB (1982) : Brain glucose bisphosphatase requires inosine monophosphate. S K Guha and Z B Rose. J. Biol. Chem 257, 6634–6637. [PubMed: 6282819]

16. Rose IA, Warms JV, and Kaklij G (1975) A specific enzyme for glucose 1,6-bisphosphate synthesis. J. Biol. Chem 250, 3466–3470. [PubMed: 235548]

17. Rose IA, Warms JV, and Wong LJ (1977) Inhibitors of glucose-1,6-bisphosphate synthase. J. Biol. Chem 252, 4262–4268. [PubMed: 558982]

18. Passonneau JV, Lowry OH, Schulz DW, and Brown JG (1969) Glucose 1,6-diphosphate formation by phosphoglucomutasein mammalian tissues. J. Biol. Chem 244, 902–909. [PubMed: 5814030]

19. Bretonnet AS, Jordheim LP, Dumontet C, and Lancelin JM (2005) Regulation and activity of cytosolic 5'-nucleotidase II. A bifunctional allosteric enzyme of the Haloacid Dehalogenase superfamily involved in cellular metabolism. FEBS Lett. 579, 3363–3368. [PubMed: 15946667]

20. Newby AC (1988) The pigeon heart 5'-nucleotidase responsible for ischaemia-induced adenosine formation. Biochem. J 253, 123–130. [PubMed: 2844163]

21. Truong VL, Collinson AR, and Lowenstein JM (1988) Evidence for the occurrence of two soluble enzymes with different substrate specificities. 121, 117–121.

22. Allen KN, and Dunaway-Mariano D (2004) Phosphoryl group transfer: evolution of a catalytic scaffold. Trends Biochem. Sci . 29, 495–503. [PubMed: 15337123]

23. Morais MC, Zhang W, Baker a S., Zhang G, Dunaway-Mariano D, and Allen KN (2000) The crystal structure of bacillus cereus phosphonoacetaldehyde hydrolase: insight into catalysis of

phosphorus bond cleavage and catalytic diversification within the HAD enzyme superfamily. Biochemistry. 39, 10385–10396. [PubMed: 10956028]

24. Peisach E, Selengut JD, Dunaway-Mariano D, and Allen KN (2004) X-ray crystal structure of the hypothetical phosphotyrosine phosphatase MDP-1 of the haloacid dehalogenase superfamily. Biochemistry. 43, 12770–12779. [PubMed: 15461449]
25. Lahiri SD, Zhang G, Dunaway-mariano D, and Allen KN (2002) Caught in the act : The structure of phosphorylated -phosphoglucomutase from Lactococcus lactis. Biochemistry. 41, 8351–8359. [PubMed: 12081483]
26. Wang W, Cho HS, Kim R, Jancarik J, Yokota H, Nguyen HH, Grigoriev IV, Wemmer DE, and Kim S-H (2002) Structural characterization of the reaction pathway in phosphoserine phosphatase: crystallographic “snapshots” of intermediate states. J. Mol. Biol 319, 421–431. [PubMed: 12051918]
27. Lu Z, Dunaway-Mariano D, and Allen KN (2008) The catalytic scaffold of the haloalkanoic acid dehalogenase enzyme superfamily acts as a mold for the trigonal bipyramidal transition state. Proc. Natl. Acad. Sci. U. S. A 105, 5687–5692. [PubMed: 18398008]
28. Burroughs a M., Allen KN, Dunaway-Mariano D, and Aravind L (2006) Evolutionary genomics of the HAD superfamily: understanding the structural adaptations and catalytic diversity in a superfamily of phosphoesterases and allied enzymes. J. Mol. Biol 361, 1003–1034. [PubMed: 16889794]
29. Zhang G, Dai J, Wang L, Dunaway-Mariano D, Tremblay LW, and Allen KN (2005) Catalytic cycling in beta-phosphoglucomutase: a kinetic and structural analysis. Biochemistry. 44, 9404–9416. [PubMed: 15996095]
30. Zhang G, Mazurkie AS, Dunaway-Mariano D, and Allen KN (2002) Kinetic evidence for a substrate-induced fit in phosphonoacetaldehyde hydrolase catalysis. Biochemistry. 41, 13370–13377. [PubMed: 12416981]
31. Dai J, Finci L, Zhang C, Lahiri S, Zhang G, Peisach E, Allen KN, and Dunaway-Mariano D (2009) Analysis of the structural determinants underlying discrimination between substrate and solvent in beta-phosphoglucomutase catalysis. Biochemistry. 48, 1984–1995. [PubMed: 19154134]
32. Wesenberg GE, Phillips GN Jr., McCoy JG, Bitto E, Bingman CA, Allard STM X-Ray Structure of Human Phosphomannomutase 2 (PMM2). PDB ID 2AMY. 10.2210/PDB2AMY/PDB
33. Lahiri SD, Zhang G, Dunaway-Mariano D, and Allen KN (2003) The pentacovalent phosphorus intermediate of a phosphoryl transfer reaction. Science. 299, 2067–2071. [PubMed: 12637673]
34. Zhang C (2008) The structural adaptation and catalytic mechanism of phosphotransferases within the haloalkanoate dehalogenase (HAD) superfamily (PhD Thesis). University of New Mexico, New Mexico, U.S.A. pg 182–185.
35. Dai J, Wang L, Allen KN, Radstrom P, and Dunaway-mariano D (2006) conformational cycling in β-phosphoglucomutase catalysis : Reorientation of the β-D-glucose 1,6-(bis)phosphate Intermediate. Biochemistry. 45, 7818–7824. [PubMed: 16784233]
36. Weeks SD, Drinker M, and Loll PJ (2007) Ligation independent cloning vectors for expression of SUMO fusions. Protein Expr. Purif 53, 40–50. [PubMed: 17251035]
37. Gonzalez A and Tsai Y (2010) A quick XDS tutorial for SSRL. Retrieved from http://smb.slac.stanford.edu/facilities/software/xds/#autoxds_script
38. Adams PD, Afonine PV, Bunkóczi G, Chen VB, Davis IW, Echols N, Headd JJ, Hung L-W, Kapral GJ, Grosse-Kunstleve RW, McCoy AJ, Moriarty NW, Oeffner R, Read RJ, Richardson DC, Richardson JS, Terwilliger TC, and Zwart PH (2010) PHENIX: a comprehensive Python-based system for macromolecular structure solution. Acta Crystallogr. D. Biol. Crystallogr 66, 213–221. [PubMed: 20124702]
39. Emsley P, and Cowtan K (2004) Coot: model-building tools for molecular graphics. Acta Crystallogr. D. Biol. Crystallogr 60, 2126–2132. [PubMed: 15572765]
40. Chen VB, Arendall WB, Headd JJ, Keedy DA, Immormino RM, Kapral GJ, Murray LW, Richardson JS, and Richardson DC (2010) MolProbity: all-atom structure validation for macromolecular crystallography. Acta Crystallogr. D. Biol. Crystallogr 66, 12–21. [PubMed: 20057044]

41. Konarev PV, Volkov VV, Sokolova AV, Koch MHJ, Svergun DI, and Koch HJ (2003) PRIMUS : a Windows PC-based system for small- angle scattering data analysis. J. Appl. Crystallogr 36, 1277–1282.
42. Svergun DI (1999) Restoring low resolution structure of biological macromolecules from solution scattering using simulated annealing. Biophys J. 76, 2879–2886. [PubMed: 10354416]
43. Dalvit C, Gossert AD, Coutant J, Piotto M (2011) Rapid acquisition of 1H and 19F NMR experiments for direct and competition ligand-based screening. Magn Reson Chem. 49, 199–202. [PubMed: 21387401]
44. Huang H, Patskovsky Y, Toro R, Farelli JD, Pandya C, Almo SC, Allen KN, and Dunaway-mariano D (2011) Divergence of structure and function in the Haloacid Dehalogenase enzyme superfamily: Bacteroides thetaiotaomicron BT2127 is an inorganic pyrophosphatase. Biochemistry. 50, 8937–8949. [PubMed: 21894910]
45. Wang W, Kim R, Jancarik J, Yokota H, and Kim S-H (2001) Crystal Structure of phosphoserine phosphatase from Methanococcus jannaschii, a hyperthermophile, at 1.8 Å resolution. Structure. 9, 65–71. [PubMed: 11342136]
46. Lahiri SD, Zhang G, Dunaway-mariano D, and Allen KN (2006) Diversification of function in the haloacid dehalogenase enzyme superfamily : The role of the cap domain in hydrolytic phosphorus-carbon bond cleavage. Bioorg. Chem 34, 394–409. [PubMed: 17070898]
47. Nguyen HH, Wang L, Huang H, Peisach E, Dunaway-mariano D, and Allen KN (2010) Structural Determinants of Substrate Recognition in the HAD Superfamily Member D-Glycero-D-manno-Heptose 1,7-bisphosphate Phosphatase, GmhB. Biochemistry. 49, 1082–1092. [PubMed: 20050614]
48. Lahiri SD, Zhang G, Dai J, Dunaway-Mariano D, and Allen KN (2004) Analysis of the substrate specificity loop of the HAD superfamily cap domain. Biochemistry. 43, 2812–2820. [PubMed: 15005616]
49. Schneidman-Duhovny D, Hammel M, Tainer JA, and Sali A (2013) Accurate SAXS profile computation and its assessment by contrast variation experiments. Biophys. J 105, 962–974. [PubMed: 23972848]
50. Schneidman-Duhovny D, Hammel M, and Sali A (2010) FoXS: a web server for rapid computation and fitting of SAXS profiles. Nucleic Acids Res. 38, W540–W544. [PubMed: 20507903]
51. Kedzierski L, Malby RL, Smith BJ, Perugini M. a, Hodder AN, Ilg T, Colman PM, and Handman E (2006) Structure of Leishmania mexicana phosphomannomutase highlights similarities with human isoforms. J. Mol. Biol 363, 215–227. [PubMed: 16963079]
52. Quental R, Moleirinho A, Azevedo L, and Amorim A (2010) Evolutionary history and functional diversification of phosphomannomutase genes. J. Mol. Evol 71, 119–127. [PubMed: 20661555]
53. Koshland DE (1995) The Key–Lock Theory and the Induced Fit Theory. Angew. Chemie Int. Ed. English 33, 2375–2378.
54. Rudolph FB, and Fromm HJ (1971) A study on the kinetics and mechanism of D-lyxose and D-xylose activation of the adenosine triphosphatase activity associated with yeast hexokinase. J. Biol. Chem 246, 2104–2110. [PubMed: 4252220]
55. Lahiri SD, Wang P-F, Babbitt PC, McLeish MJ, Kenyon GL, and Allen KN (2002) The 2.1 Å Structure of Torpedo californica creatine kinase complexed with the ADP-Mg^{2+}–NO_3^-–Creatine transition-state analogue complex. Biochemistry. 41, 13861–13867. [PubMed: 12437342]
56. Trinh CH, Asipu A, Bonthron DT, and Phillips SEV (2009) Structures of alternatively spliced isoforms of human ketohexokinase. Acta Crystallogr. D. Biol. Crystallogr 65, 201–211. [PubMed: 19237742]
57. Maryanoff BE, Neill JCO, Mccomsey DF, Yabut SC, Luci DK, Jordan AD, Masucci JA, Jones WJ, Abad MC, Gibbs AC, and Petrounia I (2011) Inhibitors of ketohexokinase: discovery of pyrimidinopyrimidines with specific substitution that complements the ATP-Binding Site. Chem. Lett 2, 538–543.
58. Cheng X-Y, Huang W-J, Hu S-C, Zhang H-L, Wang H, Zhang J-X, Lin H-H, Chen Y-Z, Zou Q, and Ji Z-L (2012) A global characterization and identification of multifunctional enzymes. PLoS One. 7, e38979. [PubMed: 22723914]
59. Jeffery CJ (1999) Moonlighting proteins. Trends Biochem. Sci 24, 8–11. [PubMed: 10087914]

60. Jacob F (1977) Evolution and tinkering. Science. 196, 1161–1166. [PubMed: 860134]
61. Zhang X, and Houk KN (2005) Why enzymes are proficient catalysts: beyond the Pauling paradigm. Acc. Chem. Res 38, 379–385. [PubMed: 15895975]
62. Afonine PV, Grosse-Kunstleve RW, Echols N, Headd JJ, Moriarty NW, Mustyakimov M, Terwilliger TC, Urzhumtsev A, Zwart PH, and Adams PD (2012) Towards automated crystallographic structure refinement with phenix.refine. Acta Crystallogr. D. Biol. Crystallogr 68, 352–367. [PubMed: 22505256]

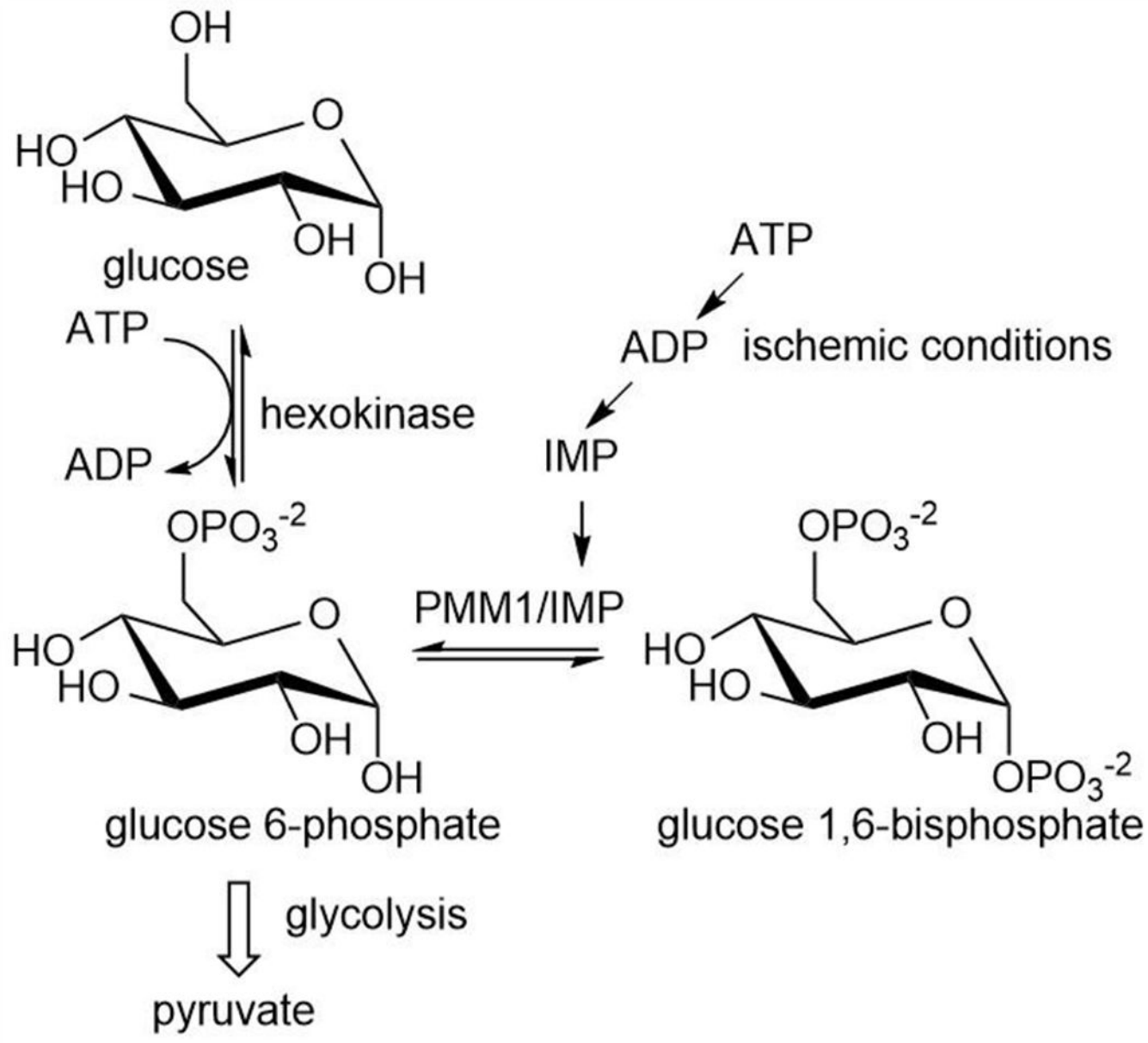

Figure 1.

Schematic of the alternate entry into glycolysis via Glu-1,6-P_2. PMM1 catalyzes hydrolysis of Glu-1,6-P_2 to Glu-6-P as cellular IMP concentration increases due to ATP depletion. This allows a temporary rescue of glycolysis by bypassing the entry step under low glucose conditions.

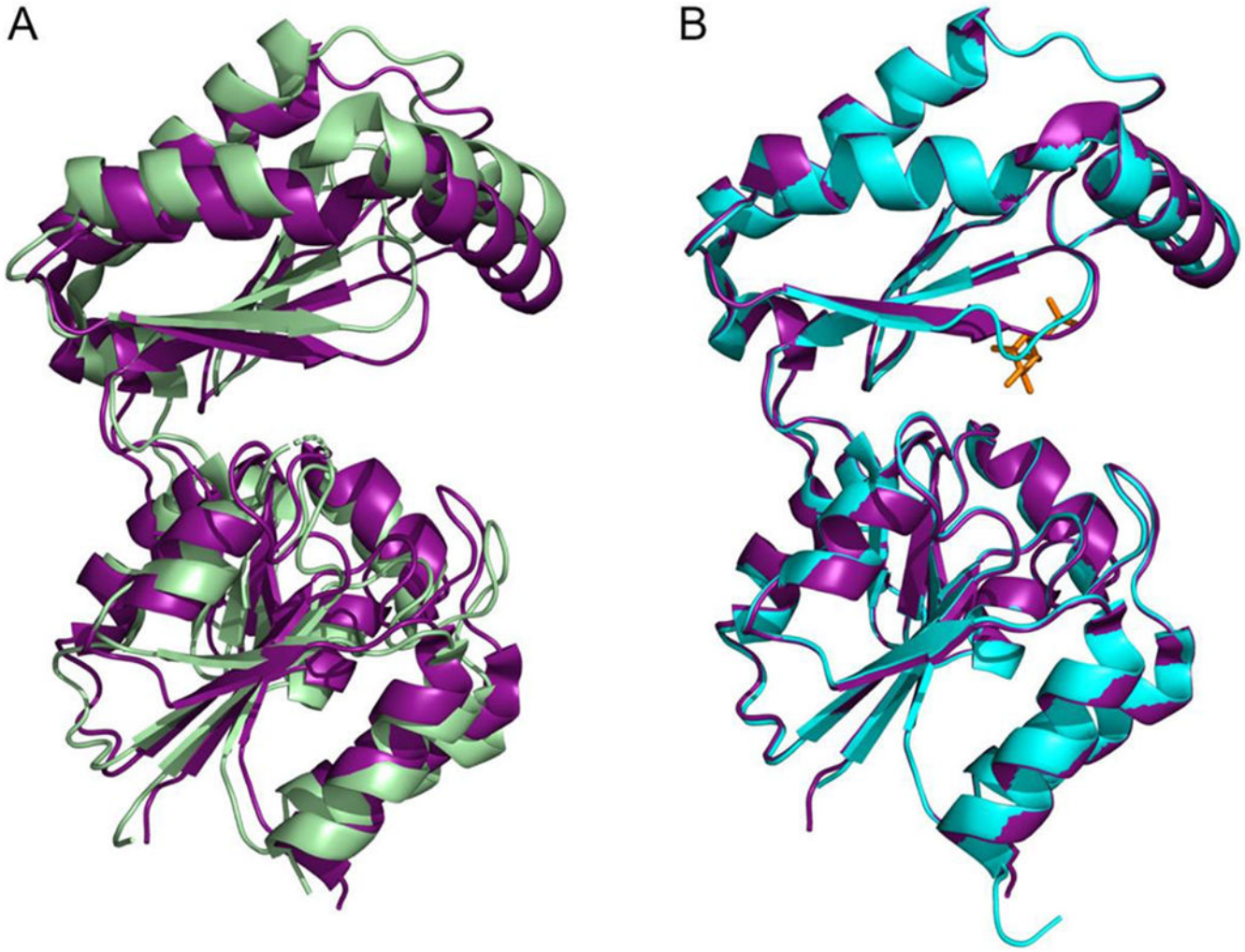

Figure 2.

Structures of human PMM isozymes (the enzyme is a homodimer, monomers are shown here as ribbon diagrams). (A) Structure of human PMM2 (PDB 2AMY, pale green) superimposed with human PMM1 (PDB 2FUC, purple). The rmsd between PMM2 and unliganded PMM1 is 0.646 Å for the cap and 1.56 Å for the core domain. (B) Superimposition of unliganded PMM1 (PDB 2FUC, purple) and PMM1 bound to Man-1-P (orange sticks) (PDB 2FUE, cyan). The two structures have an rsmd of 0.53 Å.

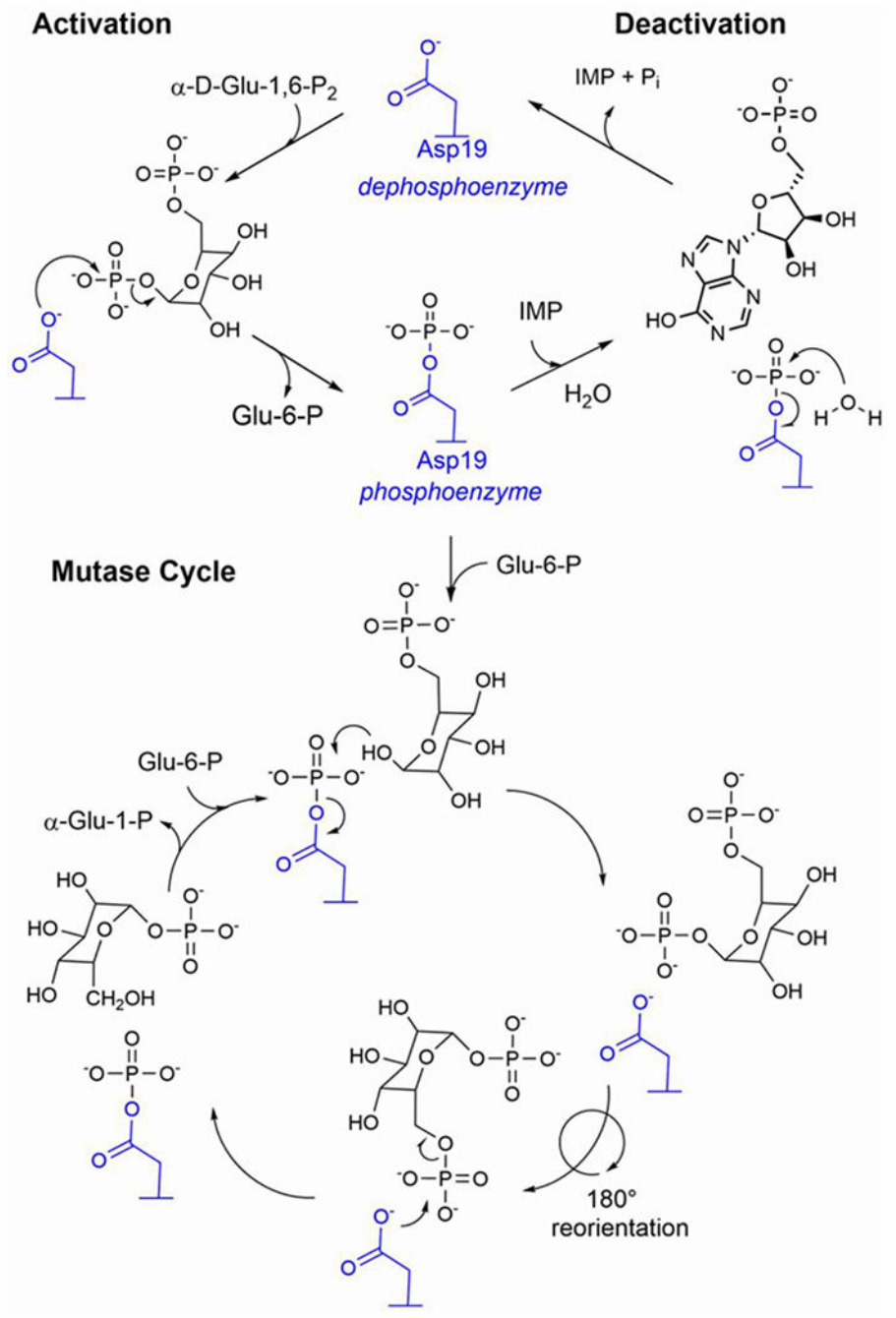

Figure 3.

Proposed mechanism of catalysis in PMM mutase and phosphatase activity (shown here for PMM1). Both mechanisms are initiated by the phosphoryl transfer from a bisphosphorylated sugar, Glu-1,6-P_2 or Man-1,6-P_2, to the aspartyl nucleophile, Asp19 (activation). As a phosphatase (in the presence of IMP), PMM1 accepts Glu-1,6-P_2 as a substrate to produce Glu-6-P (or Glu-1-P) and P_i (deactivation). In the case of the mutase function, Glu-1,6-P_2 or Man-1,6-P_2 (shown here for glucose) serves as the coactivator to produce the phosphorylated form of the protein and accepting monophosphorylated hexose as the

substrate (mutase cycle). PMM2 does not undergo IMP mediated deactivation although hydrolysis of the phosphoenzyme still occurs.

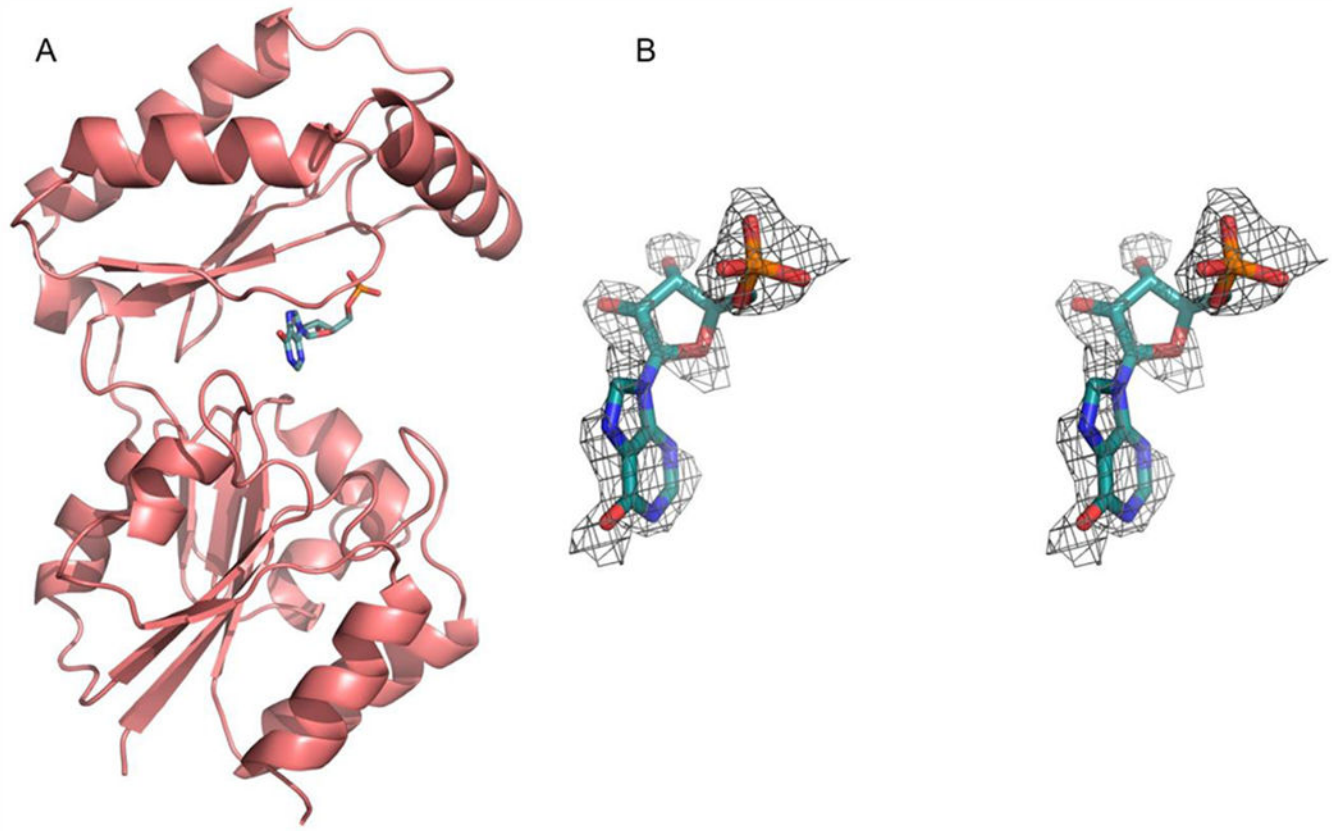

Figure 4.

Structure of IMP bound to the cap domain of PMM1. (A) Cartoon representation of PMM1 (salmon) in complex with IMP (teal) and (B) stereo view of electron density of IMP from simulated annealing composite omit $2F_o - F_c$ map contoured at 1.0σ level (gray wire frame). The image was rendered using PyMOL.

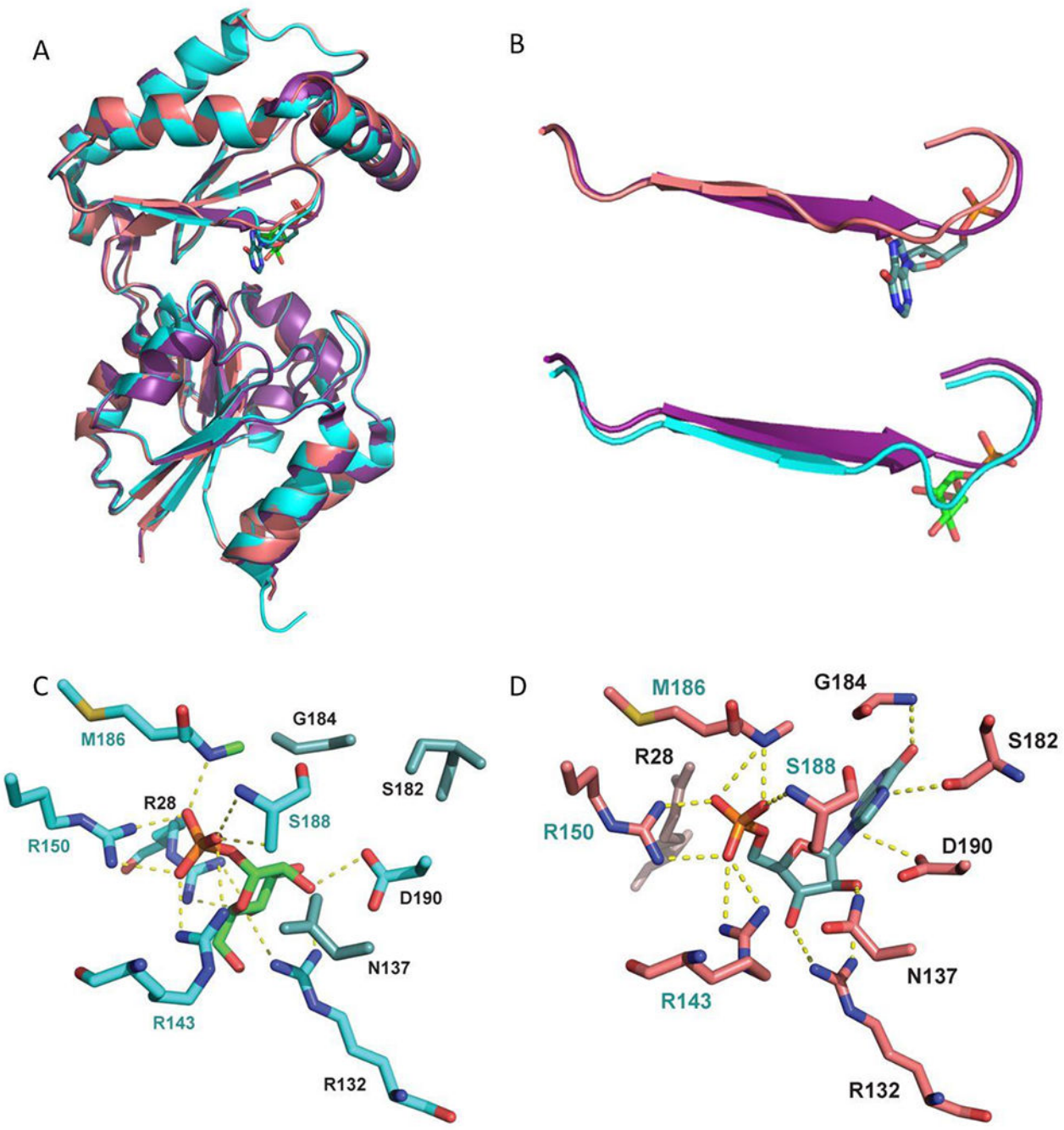

Figure 5.

Comparison between unliganded PMM1 and PMM1 in complex with substrate Man-1-P and activator IMP. (A) Overlay of unliganded PMM1 (2FUC, purple), PMM1 bound to Man-1-P (2FUE, cyan) and PMM1 bound to IMP (salmon) are shown as cartoons, IMP (teal) and Man-1-P (green) are shown as sticks. The two structures are similar with rmsd of 0.37 Å and 0.55 Å of Man-1-P bound PMM1 and IMP bound PMM1 relative to unliganded PMM1, respectively. (B) The distal phosphate binding loop showing the disruption of β-strand due to IMP binding (top) and Man-1-P binding (bottom). (C and D) Residues within hydrogen-

bonding distance of Man-1-P (C) and IMP (D). Residues labeled in blue form hydrogen bonds with the phosphoryl moiety of ligand and residues labeled in black form hydrogen bonds to either the sugar (C) or nucleotide (D) moiety of ligand. Residues that are colored dark teal in (C) and dark pink in (D) do not participate in hydrogen bonding to the respective ligands.

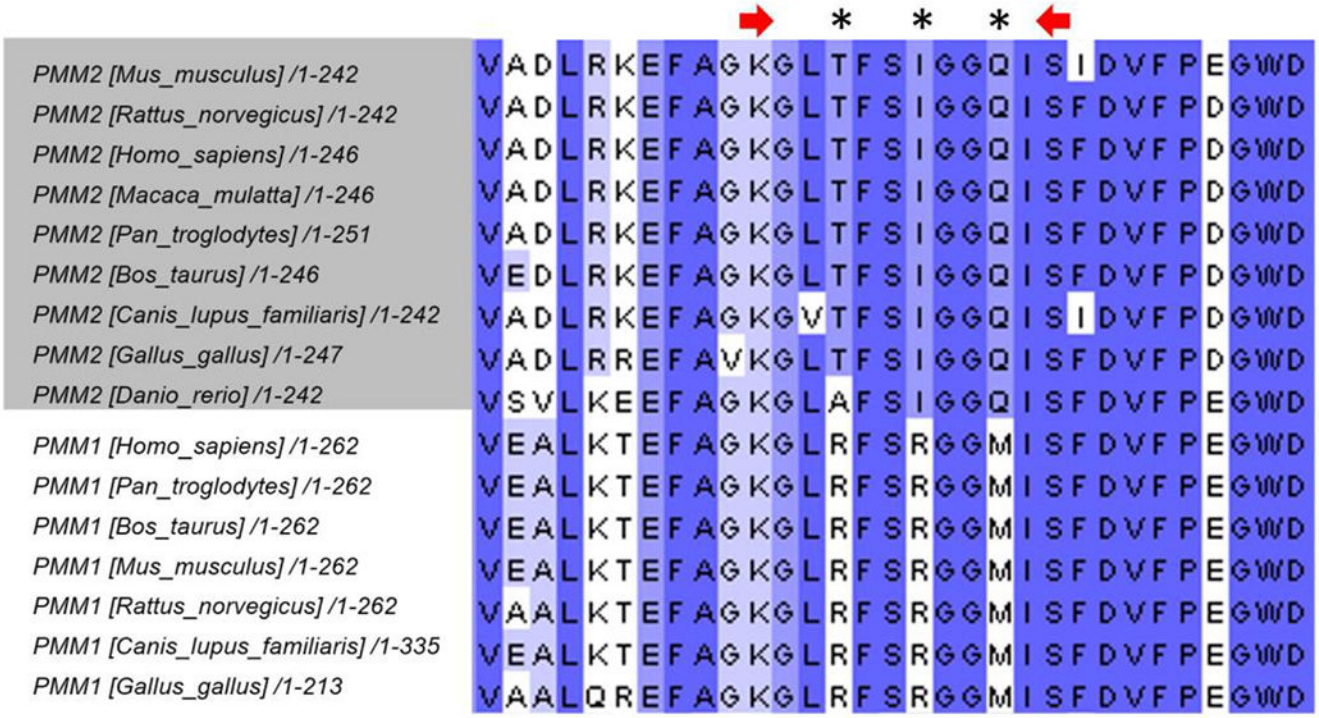

Figure 6.

Sequence alignment of PMM2 (top) and PMM1 (bottom). Residues between the red arrows are the residues located at the β8-strand. Asterisks indicate the conserved differences between PMM1 and PMM2, where residues T171, T174, and Q177 of human PMM2 are conserved within PMM2 orthologs and R180, R183, and M186 are conserved in PMM1 orthologs.

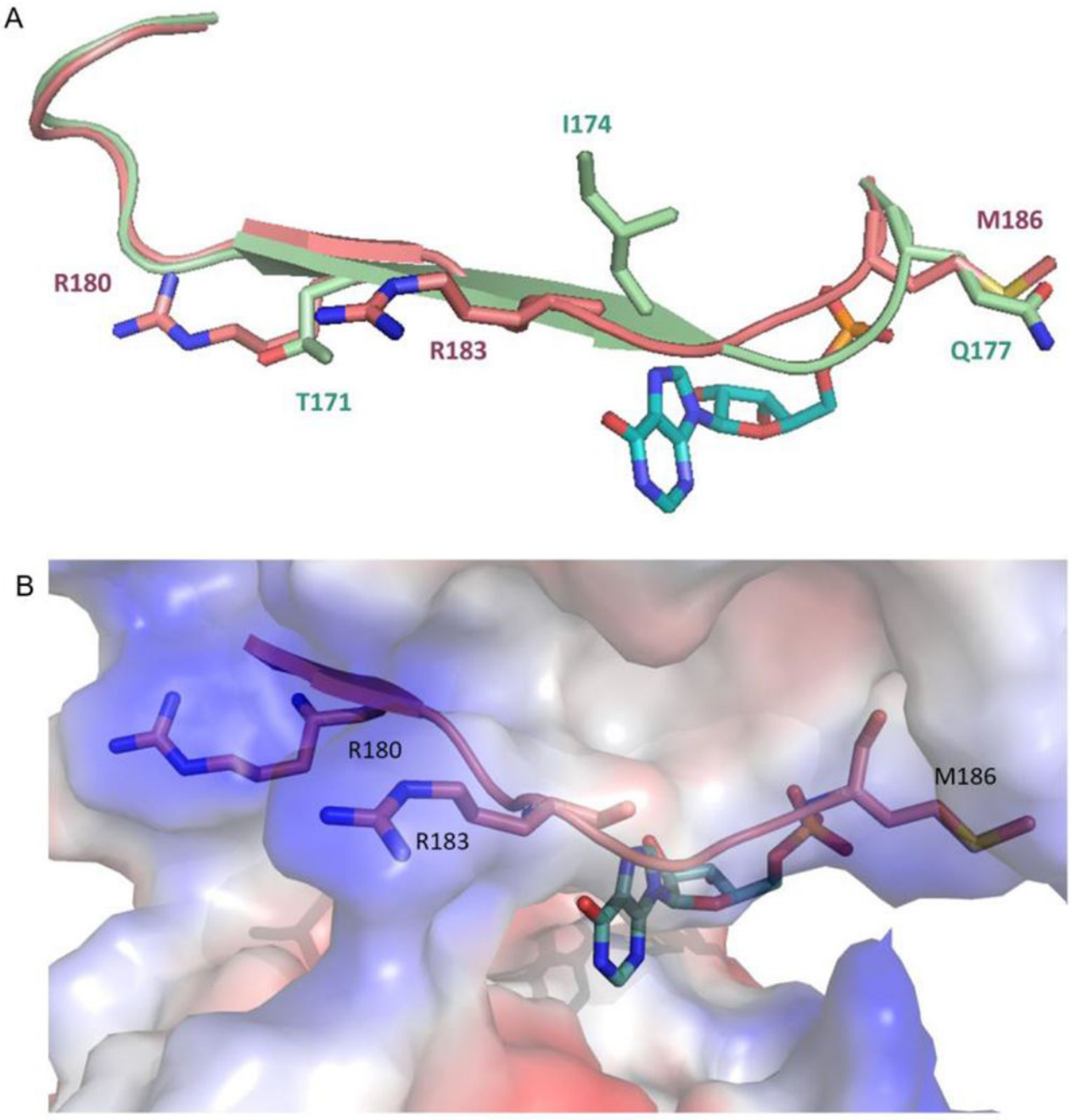

Figure 7.

Ligand-binding loops of PMM1 and PMM2 (A) The loop from the structure of PMM2 liganded to Man-1-P (light green, 2FUE) superimposed with that from PMM1 (salmon) liganded to IMP (cyan sticks) with the loop displayed as cartoon and residues that differ from PMM2 shown as sticks. (B) PMM1 liganded to IMP (salmon) with residues that differ from PMM2 and IMP shown as sticks and the calculated protein molecular electrical potential displayed as a semitransparent surface (colored from red (−5 kT/e) to blue (+5 kT/e)).

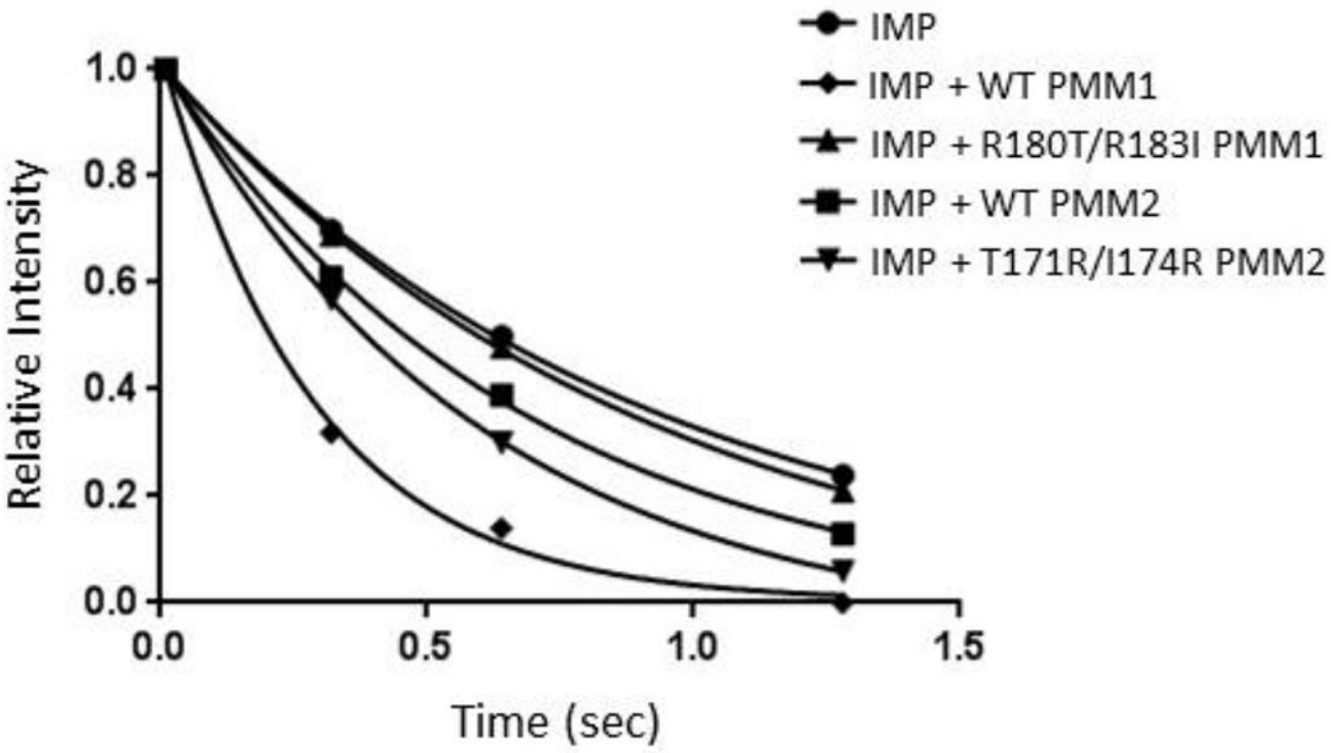

Figure 8:

T2 relaxation curves for IMP alone and in presence of PMM variants. Time indicated on the x-axis is the relaxation time delay at which signal intensity is measured during the NMR experiment. Curves were fitted using a one phase exponential decay equation, $Y = (Y_0 - NS)*\exp(-k*X) + NS$, where Y_0 is the binding at time zero, NS is the binding at infinite time, and k is the rate constants in inverse units of the x-axis. Curves were generated using GraphPad Prism. All experiments used 50 μM protein and 0.9 mM IMP ligand.

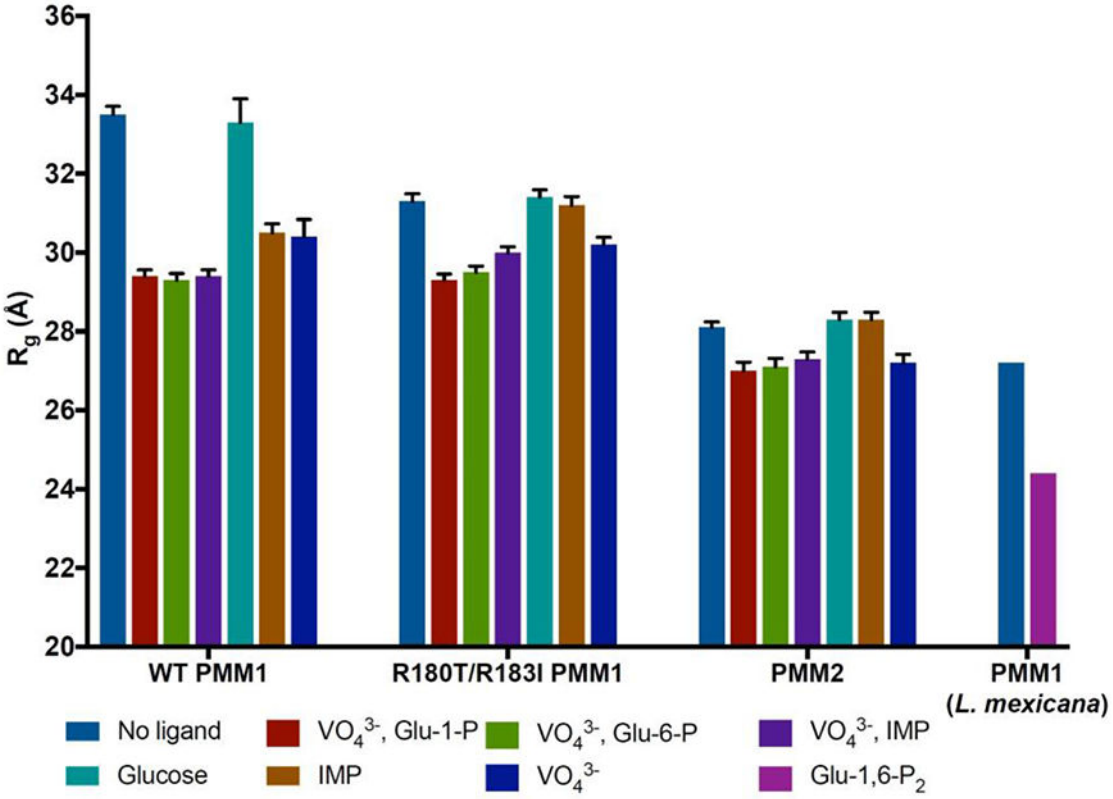

	WT PMM1	R180T/R183I PMM1	WT PMM2
no ligand	33.5 ± 0.21	31.3 ± 0.19	28.1 ± 0.14
VO_4^{3-}, Glu-1-P	29.4 ± 0.16	29.3 ± 0.16	27.0 ± 0.22
VO_4^{3-}, Glu-6-P	29.3 ± 0.17	29.5 ±0.16	27.1 ± 0.22
VO_4^{3-}, IMP	29.4 ± 0.16	30 ± 0.15	27.3 ± 0.18
Glucose	33.3 + 0.60	31.4 ± 0.19	28.3 ± 0.19

Figure 9:

Radius of gyration (Rg (Å)) determined from SAXS data on wild-type PMM1 (WT PMM1) and PMM2 and R180T/R183I PMM1. Data was collected using 10 mg/mL protein and 10 mM ligand (see legend for ligand identity). Note that the values for *L. mexicana* PMM1 are calculated from the corresponding PDB files (unliganded, PDB 2I54 and Glu-1,6-P_2 liganded, PDB 2I55) using the program FOXS.

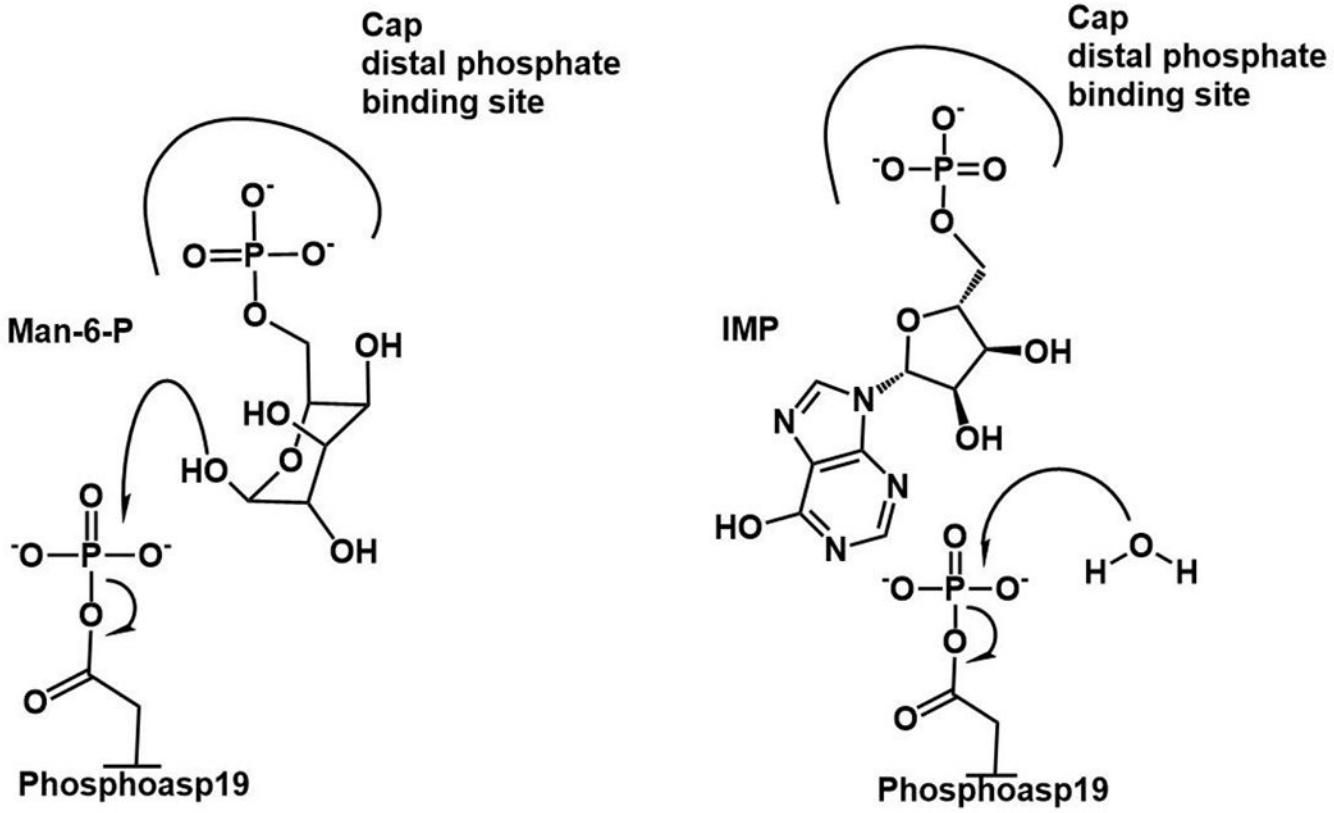

Figure 10:

Model for PMM1 mutase versus phosphohydrolase mechanisms. The hypothesis is that the mutase activity (left) and the phosphatase activity (right) share the phosphoenzyme intermediate and enzyme conformer where the binding molecule induces cap closure. In the mutase mechanism, a molecule of Man-6-P (or Man-1-P) binding to the cap domain allows for proper alignment with the phosphoaspartate intermediate for phosphoryl transfer to generate the Man-1,6-P_2 intermediate. Although IMP does initiate cap closure, it does not interact with the phosphoaspartate. Instead, a water molecule serves as a nucleophile to generate phosphate.

Table 1.

Crystallographic data collection and model refinement statistics for PMM1/IMP complex.

Data Collection	
PDB ID	6CFV
Space group	P 4_3 2_1 2
Unit cell	
a=b, c (Å)	52.2, 214.5
Resolution range [a] (Å)	34.88 - 1.92 (1.99 - 1.92)
R-merge	0.0148 (0.156)
R-meas	0.0209
Mean I/σ(I)	30.3 (5.01)
Model Refinement [b]	
Total reflections	45844 (3720)
Unique reflections	23377 (1975)
R-work	0.1698 (0.2034)
R-free[c]	0.224 (0.248)
Multiplicity	2.0 (1.9)
Completeness (%)	98.20 (85.02)
Number of atoms	2301
macromolecules	1969
ligands	25
water	307
R.M.S. deviations	
Bond lengths (Å)	0.007
Bond angles (°)	1.05
Clashscore	14.12
Average B-factor	24.1
macromolecules	22.6
ligands	
IMP	38.8
Mg^{2+}	21.3
solvent	32.7
Ramachandran	
favored (%)	97.5
allowed (%)	2.5

[a] Values in parenthesis relate to the highest-resolution shell.

[b] Calculated by PHENIX.refine using the formula described in Afonine *et al.*[62]

[c] The R_{free} test set size was 8.6%.

Table 2.

The steady-state kinetic constants and inhibition dissociation constants for IMP measured for wild-type PMM1 (WT PMM1), PMM1 variants, and PMM2 for mutase activity converting Glu-1-P to Glu-6-P (see Materials and Methods). ND = no activity detected

Protein	Kinetic constants for Mutase Activity			
	k_{cat} (s^{-1})	K_m (μM)	k_{cat}/K_m ($M^{-1}s^{-1}$)	K_i^{IMP} μM
WT PMM1[a]	1.3 ± 0.045	19 ± 2.1	6.8×10^4	2.0 ± 0.31
R180T/R183I PMM1	1.6 ± 0.055	17 ± 2.1	9.4×10^4	780 ± 47
R183I PMM1	1.0 ± 0.020	8.0 ± 0.74	1.3×10^5	350 ± 25
R180T PMM1	0.9 ± 0.030	28 ± 2.8	3.2×10^4	2.3 ± 0.24
M186Q PMM1	1.1 ± 0.063	10 ± 2.1	1.1×10^5	2.8 ± 0.28
R108K/R183K PMM1	2.1 ± 0.19	13 ± 3.9	1.6×10^5	2.0 ± 0.30
WT PMM2[a]	1.0 ± 0.058	8.0 ± 1.8	1.3×10^5	> 4000
T171R/I174R PMM2	ND	ND	ND	

[a]Also previously measured in [1,2]

Table 3.

The steady-state kinetic constants measured for wild-type PMM1 (WT PMM1), PMM1 variants and PMM2 for phosphatase activity converting Glu-1,6-P_2 to Glu-6-P (see Materials and Methods). ND = no activity detected

	Kinetic constants for phosphatase activity (− IMP)				
	k_{cat} (s^{-1})	**K_m (μM)**	**k_{cat}/K_m ($M^{-1}s^{-1}$)**		
WT PMM1	0.018 ± 0.0012	18 ± 3.4	1.0 x 10^3		
R180T/R183I	0.022 ± 0.0009	54 ± 7.2	4.0 x 10^2		
R183I	0.011 ± 0.0004	16 ± 1.8	6.7 x 1 0^2		
R180T	0.024 ± 0.0012	14 ± 2.4	1.7 x 10^3		
M186Q	0.014 ± 0.0008	14 ± 2.7	1.0 x 10^3		
R108K/R183K	0.028 ± 0.0017	13 ± 2.7	1.5 x 10^3		
WT PMM2	ND	ND	ND		
	Kinetic constants for phosphatase activity (+ IMP)				
	k_{cat} (s^{-1})	**K_m (μM)**	**k_{cat}/K_m ($M^{-1}s^{-1}$)**	**K_{act}^{IMP} (μM)**	**[IMP]**
WT PMM1	1.4 ± 0.092	8.5 ± 1.6	1.6 x 10^5	1.5 ± 0.21	100 μM
R180T/R183I	0.16 ± 0.006	21 ± 2.6	7.6 x 10^3	760 ± 155	2 mM
R183I	1.1 ± 0.045	10 ± 1.7	1.1 x 10^5	180 ± 28	2 mM
R180T	3.1 ± 0.13	17 ± 2.1	1.8 x 10^5	14 ± 2.8	100 μM
M186Q	3.5 ± 0.25	19 ± 4.0	1.8 x 10^5	7.0 ± 1.8	100 μM
R108K/R183K	2.2 ± 0.096	13 ± 1.9	1.7 x 10^5	1.9 ± 0.27	100 μM
WT PMM2	ND	ND	ND	---	2 mM